2024

Neural compensation in response to salinity perturbation in the cardiac ganglion of the American lobster, *Homarus americanus*

Josephine P. Tidmore
Bowdoin College

Neural compensation in response to salinity perturbation in the cardiac ganglion of the American lobster, *Homarus americanus*

An Honors Project for the Program of Neuroscience

By Josephine P. Tidmore

Bowdoin College, 2024

TABLE OF CONTENTS

ACKNOWLEDGEMENTS

Over the past four years at Bowdoin, I have had the good fortune of working with talented scientists who inspire me and from whose mentorship and support I will continue to benefit. First, I would like to thank my advisor, Professor Dan Powell, for his guidance from the conception to the completion of this project. I am immensely grateful to have had the opportunity to learn and grow under his tutelage.

I am thankful to Professor Dave Schulz and Virginia Garcia at the University of Missouri-Columbia, who welcomed me into the Schulz Lab and without whom this project would not have been possible. I am indebted to Professor Patsy Dickinson for providing me with the foundation to conduct this research and for her mentorship that has enabled my growth as a scientist. Having never met me in-person, she generously accepted me into her lab the summer after my first year, and it was this introduction to independent research that ignited my interest in neuroscience.

I thank my lab mates—past and present—for their advice, support, and friendship. To Grant, Karin, and Katrina: thank you for your encouragement, for the laughter and memories, in and outside of the lab. I am so glad we did this together. To my friends and family, thank you for your love and for the phone calls that sustained me through many long hours of pulling cells. I love you all.

Lastly, this research would not have been possible without funding from the Paller Neuroscience 2023-2024 Academic Year Fellowship, the Bowdoin College Fall Research Award and Grua/O'Connell Mini Grant, and the Maine IDeA Network of Biomedical Research Excellence (NIH-NIGMS 8P20GM0103423-12).

ABSTRACT

Central pattern generator (CPG) networks produce the rhythmic motor patterns that underlie critical behaviors such as breathing, walking, and heartbeat. The fidelity of these neural circuits in response to fluctuations in environmental conditions is essential for organismal survival. The specific ion channel profile of a neuron dictates its electrophysiological phenotype and is under homeostatic control, as channel proteins are constantly turning over in the membrane in response to internal and external stimuli. Neuronal function depends on ion channels and biophysical processes that are sensitive to external variables such as temperature, pH, and salinity. Nonetheless, the nervous system of the American lobster (*Homarus americanus*) is robust to global perturbations in these variables.

The cardiac ganglion (CG), the CPG that controls the rhythmic activation of the heart in the lobster, has been shown to maintain function across a relatively wide, ecologically-relevant range of saline concentrations in the short-term. This study investigates whether individual neurons of the CG sense and compensate for long-term changes in extracellular ion concentration by controlling their ion channel mRNA abundances. To do this, I bathed the isolated CG in either 0.75x, 1.5x, or 1x (physiological) saline concentrations for 24 h. I then dissected out individual CG motor neurons, the pacemaker neurons, and sections of axonal projections and used single-cell RT-qPCR to measure relative mRNA abundances of several species of ion channels in these cells.

I found that the CG maintained stable output with 24 h exposure to altered saline concentrations (0.75x and 1.5x), and that this stability may indeed be enabled by changes in mRNA abundances and correlated channel relationships.

INTRODUCTION

Central pattern generator (CPG) networks produce the neural rhythms that underlie crucial motor behaviors such as breathing and locomotion as well as essential functions like heartbeat and chewing (Delcomyn, 1980). CPGs are present in nervous systems across taxa, and the number of neurons comprising these networks can vary dramatically. In invertebrate species like lobsters and crabs, a handful of neurons drive rhythmic feeding behavior (Marder & Bucher, 2007); in vertebrates, large assemblies of thousands of neurons in the spinal cord coordinate locomotion (Goulding, 2009). A defining feature of CPGs is their ability to independently produce patterned electrical activity in the absence of external timing cues; that is, without sensory feedback from central or peripheral inputs (Marder & Bucher 2001). Because of their small size and known connectivity, invertebrate CPGs are particularly tractable systems that allow us to understand basic neural principles through simple experimental manipulations.

CPGs must be able to reliably produce patterned activity necessary for essential, stereotyped behaviors in an organism. The fidelity of these networks in response to environmental stimuli is, therefore, essential for organismal survival. Accumulating experimental observations from CPGs in crab species have suggested that these networks are robust to global perturbations in external variables such as ambient temperature (Tang et al., 2010, 2012; Rinberg et al., 2013; Soofi et al., 2014; Haddad & Marder, 2018; Ratliff et al., 2021), pH (Haley et al., 2018; Ratliff et al., 2021), and extracellular ion composition (He et al., 2020; Rue et al., 2022). These global perturbations are environmental challenges that influence all neurons of a circuit and, in some cases, all biophysical processes of a cell. For example, experiments using the stomatogastric nervous system (STNS), a CPG network in the crab, found that this system remains functional within an ecologically-relevant range of perturbations in temperature and pH. Tang et al. (2010) reported that performance of the pyloric network—a subnetwork within the

crustacean STNS—is robust to a temperature range of 7°C to 23°C in the short-term (CPG robustness refers to the continued generation of behaviorally-relevant cyclic patterns of neural activity). Similarly, computational models of a pyloric network found that the duty cycle (proportion of time the circuit is active) and triphasic pyloric rhythm is maintained across a range of temperatures (10°C to 25°C), suggesting stable functional output with altered temperature (Alonso & Marder, 2020).

Neuronal homeostatic plasticity

Understanding how a circuit maintains functionality despite environmental perturbation relies on an understanding of how stability is achieved at an individual cellular level. The cell's ability to sense information from external stimuli and integrate this information to produce altered activity in response to changes in the environment is referred to as homeostatic plasticity (Turrigiano and Nelson, 2004; Northcutt & Schulz, 2019). A single neuron is a homeostatic system with a "set point" that defines its output such that, in response to perturbation, deviation from the set point is sensed and compensatory feedback programs are initiated to reestablish the set point (Davis, 2006). A cell can modulate its excitability to reach a certain activity set point by adjusting several parameters, such as synaptic strength (Turrigiano & Nelson, 2004), neurotransmitter release (Paradis et al., 2001), receptor sensitivity on the postsynaptic membrane (David & Goodman, 1998), and ion channel density (Baines, 2005; O'Leary, 2018).

The specific ion channel profile of a neuron dictates its electrophysiological phenotype and is dynamically controlled by the cell. More than 300 distinct ion channels have been identified in the mammalian genome (Tanner & Beeton, 2018), and even "simple" nervous systems, like that of the American lobster *Homarus americanus*, contain tens of different ion channel genes (Northcutt et al., 2016). Considering all possible permutations of a given ion

channel due to alternative splicing and post-translational modification increases the functional expression patterns by many orders of magnitude (Lin et al., 2012; Lipscombe et al., 2013). A possible explanation for the purpose of such an array of ion channels is that multiple ion channels are required for a neuron to compensate for environmental perturbations and biological variability, thereby allowing for flexibility and robustness of physiological function (O'Leary and Marder 2016; Alonso and Marder, 2019). The homeostatic capacity of a neuron may be explained by two types of compensation that operate on different timescales: the first type arises from the "degeneracy" of ion channels, and the second type of compensation relies on activity-dependent feedback, a type of homeostatic plasticity (O'Leary, 2018).

Ion channel degeneracy

The variety of ion channels gives rise to overlap in channel function, or degeneracy. For instance, several different potassium currents contribute to spike repolarization in a neuron, despite differences in their voltage and time dependencies (Golowasch et al., 1992; Drion et al., 2015; Goaillard & Marder, 2021). The idea that several ion channels can substitute functionally for one another supports observations from computational models which show that disparate circuit parameters (e.g., different channel densities) can underlie similar neuronal and network behavior (Prinz et al., 2004; O'Leary et al., 2013; Alonso & Marder, 2019). Indeed, several studies have demonstrated two- to six-fold variability in intrinsic parameters of individual identified neurons across individuals in the same species (Schulz et al., 2006, 2007; Tobin et al., 2009; Norris et al., 2011; Northcutt et al., 2019). This variability is seen in ion channel conductance and gene expression across animals with similar neural output, implying that there are multiple solutions to achieve the same target activity. Despite this variability, clear linear correlations between channel expression patterns are observed, suggesting that functional

relationships between certain ion channels are required for normal neuronal activity (Schulz et al., 2007; Temporal et al., 2012; O'Leary et al., 2013). If, indeed, it is these correlated channel relationships that define neuronal activity states, then the homeostatic set point of a neuron need not be a static value but, instead, is permitted to vary (i.e., noisy expression patterns will not silence the neuron).

Channel degeneracy is thought to contribute to short-term neuronal and network stability in response to perturbations. For example, the expression of multiple types of K^+ or Ca^{2+} currents with overlapping activation/inactivation characteristics in a single neuron may permit adaptation to perturbations, as the relative contribution of these currents to spiking behavior is flexible and can change in response to cues like membrane potential or temperature (Golowasch et al., 1992; Marom & Marder, 2023). As a result, degenerate ion channels give rise to functional adaptation without the need for channel protein biosynthesis or altered gene transcription, allowing for innate compensation in response to environmental stimuli.

Activity-dependent feedback

Activity-dependent feedback (homeostatic plasticity), on the other hand, is responsible for neuron self-tuning over longer timescales because, as previously described, it involves sensing an activity set point and homeostatically regulating channel expression to return to the set point, maintaining a functional configuration following perturbation. In this model, changes in neuronal activity feed back to alter transcription, resulting in homeostatic regulation of intrinsic excitability through manipulation of a neuron's channel densities. Evidence for this in biological neurons has come from studies in cultured neurons from both invertebrate and vertebrate nervous systems, where neurons that had been incubated with tetrodotoxin (TTX) for several days to silence their activity displayed increased sensitivity to current injection when

TTX was washed out. This increased excitability was due to selective regulation of Na^+ and K^+ conductances, leading to an increase in Na^+ and decrease in K^+ channel density (Turrigiano et al., 1994; Desai et al., 1999). Another study which used a genetic knockout model to study responses to the long-term reduction in voltage-dependent sodium conductance showed that Purkinje neurons have long-term feedback mechanisms that permit maintenance of firing despite reduction in sodium current (Swensen & Bean, 2005). Similarly, computational models in which specific ion conductances are deleted show neural compensation over long timescales and simulate CPG networks' ability to regulate ion channel transcription and translation to maintain homeostasis (O'Leary et al., 2014). These studies, and many others, have demonstrated that slow, activity-dependent feedback mechanisms allow neurons to change their intrinsic properties by modulating channel densities to compensate for various perturbations in the long-term.

Calcium-mediated signaling cascades

Transcriptional control of ion channels is thought to be regulated by calcium signaling, where the influx of calcium ions in response to neural activity results in downstream gene activation or suppression as mediated by master transcription factors (Figure 1). Intracellular calcium concentration—which can be altered through the opening of voltage-gated Ca^{2+} channels—acts as an activity sensor, which then relays signals to the nucleus to regulate ion channel transcription. Many transcription factors, like cAMP-responsive element binding protein (CREB), are known to be Ca^{2+}-dependent or dependent on other Ca^{2+}-sensing molecules, implying that mRNA production is also calcium-dependent (Finkbeiner & Greenberg, 1998; Mermelstein et al., 2000). In fact, membrane depolarization has been linked to CREB phosphorylation (i.e., activation) and gene expression in studies in primary cultures of SGG and hippocampal neurons (Wheeler et al., 2012). Computational models that incorporate the

assumption that ion channel mRNA production rate is Ca^{2+}-dependent can simulate a neuron whose average intracellular Ca^{2+} concentration encodes an increase or decrease in activity, where the resultant activity-dependent regulation of conductance restores bursting behavior (O'Leary et al., 2014).

Because neural activity can be modulated by calcium concentration, which, in turn, initiates activity-dependent feedback pathways controlling ion channel expression, it is plausible that the neurons of a simple crustacean CPG—the lobster cardiac ganglion—can compensate for changes in extracellular concentration of calcium and other ions. I hypothesized that individual neurons exposed to global challenges in extracellular ionic concentrations may be able to sense changes salinity and adjust their mRNA abundances in response in order to permit the system to maintain its functional output over a longer timescale.

The lobster cardiac ganglion

The cardiac ganglion (CG) of the American lobster (*H. americanus*) is a useful model to study the response to changes in salinity on a cellular and system level (Cooke 2002). The CG is a simple, nine-neuron oscillator composed of five motor neurons (or large cells, LC) and four pacemaker premotor neurons (or small cells, SC) that control the rhythmic activation of the heart. These neurons are electrochemically coupled, and their synchronous activity underlies rhythmic heart contractions in the animal. The anatomical and electrophysiological properties of this network have been well-characterized, and the set of ion channels expressed by neurons of the CG are also known and can be characterized through molecular approaches.

Do neurons sense and compensate for changes in extracellular ionic concentration?

The present study aims to investigate long-term compensation in response to salinity perturbation in a simple crustacean CPG neural circuit. While many studies in crustacean CPGs

(as mentioned above) have examined robustness to other perturbations like temperature, the effect of global salinity perturbation has not been well-characterized. Unpublished data has suggested that this system can maintain function across a relatively wide, ecologically-relevant salinity range in the short-term; however, whether this maintenance of function can be achieved as a result of adaptive changes in ion channel expression has not been studied.

To investigate this question, I exposed cardiac ganglion preparations to two altered salinity concentrations (0.75x and 1.5x) for a period of 24 h, long enough to elicit changes in the CG's motor output and to observe substantial changes in ion channel mRNA abundances. I then dissected out individual motor neurons, the pacemaker neurons, and sections of axonal projections and used single-cell quantitative reverse transcription polymerase chain reaction (RT-qPCR) to measure relative mRNA abundances for several ion channel species in these cells.

MATERIALS & METHODS

Animals

Female and male adult American lobsters (*Homarus americanus*) were obtained from local seafood retailers (Brunswick, ME, USA). Animals were housed in recirculating natural seawater aquaria at 10-12°C on a 12hr:12hr light-dark cycle and were fed a diet of chopped fish and squid. Individual lobsters were anesthetized by packing in ice for 30 min before isolation of the heart from the cephalothoracic carapace via manual microdissection in chilled (8–10°C) physiological saline.

Isolated cardiac ganglion preparations

The cardiac ganglion (CG) was isolated by opening the heart along the ventral axis, and the trunk and anterolateral nerves of the CG were dissected from the surrounding musculature (Figure 2). The ganglion was pinned (ventral side up) to a clear, Sylgard-lined dish and superfused with cold (10°C) physiological saline at a flow rate of approximately 5 mL/min using a Rabbit peristaltic pump (Gilson, Middleton, WI). Temperature of the bath was continuously monitored and maintained at approximately 10°C using an in-line temperature regulator (CL-100 bipolar temperature controller and SC-20 solution heater/cooler; Warner Instruments) with a temperature probe (Warner Instruments, Hamden, CT, USA).

Saline solutions

Physiological (control) *H. americanus* saline was composed of 479.12 mM NaCl, 12.74 mM KCl, 13.67 mM $CaCl_2$, 20.00 mM $MgSO_4$, 3.91 mM Na_2SO_4, 11.45 mM Trizma base, and 4.82 mM maleic acid. 1.5x and 0.75x saline solutions were prepared by altering the amount of sterile deionized water (diH_20) in which the salts were dissolved. All saline solutions had pH 7.45 at 23°C. These concentrations were chosen because preparations reliably functioned after 24 h of exposure (data not shown).

Experimental groups

Motor neurons (large cells, LC) and premotor neurons (small cells, SC) as well as a section of axon containing no neurons of the CG were collected from four different experimental groups; 1) *Control* (LC1 *N*=10; LC2 *N*=10; LC3 *N*=8; LC4 *N*=10; LC5 *N*=9; SC *N*=10; Axon *N*=10): these isolated CG preparations were exposed to 1x *H. americanus* saline for a period of 24 h. 2) *0.75x saline* (LC1 *N*=10; LC2 *N*=9; LC3 *N*=8; LC4 *N*=9; LC5 *N*=8; SC *N*=10; Axon *N*=10): these preparations were exposed to 0.75x saline for 24 h. 3) *1.5x saline* (LC1 *N*=10; LC2 *N*=10; LC3 *N*=9; LC4 *N*=10; LC5 *N*=10; SC *N*=10; Axon *N*=10): these CG preparations were exposed to 1.5x saline for 24 h. 4) *Acute control* (LC1 *N*=10; LC2 *N*=10; LC3 *N*=10; LC4 *N*=10; LC5 *N*=8; SC *N*=10; Axon *N*=10): cells from these preparations were collected <1 h after dissection.

For all groups (excluding acute control), the saline in the dish was replaced with saline containing 1g/L D-glucose to ensure the health of preparations for 24 h experiments. Preparations were covered and kept at 4°C for 24 h. Only cells from two experimental groups (1x saline for 24 h and 0.75x saline for 24 h) were used for the qPCR experiments described in this study.

Electrophysiology

Extracellular nerve recordings were sampled immediately upon dissection of the CG in physiological saline for each preparation in each experimental group to obtain a baseline recording of neural activity. Large and small cell action potentials were recorded using stainless steel bipolar pin electrodes, isolated from the bath with a petroleum jelly well built around the CG trunk. One pin was placed inside the well to record motor output from the CG, while the other pin was placed just outside the well in the bath. Neuronal output was amplified using a

Model 1700 A-M Systems Differential AC Amplifier (Sequim, WA) and was then digitized at 10 kHz using a CED Micro 1401 USB interface and Spike2.0 v9.01 data acquisition software (Cambridge Electronic Design, Cambridge, UK) on a Dell PC (Dell, Austin, TX). Recordings were taken from preparations in the altered saline groups after 10 min of superfusion with either 1.5x or 0.75x saline. Recordings were then taken at the 24 h time point for all preparations (excluding acute controls) prior to cell harvesting.

Intracellular voltage measurements were taken from one of the motor neurons (LC2; N=1). The cell body was exposed by removing the protective sheath surrounding the motor neurons. Neurons were impaled using a bridge-balanced glass microelectrode (R=15-35 MΩ) filled with squid cytoplasmic solution (20 mM NaCl, 15 mM Na_2SO_4, 10mM Hepes, 400 mM potassium gluconate, and 10 mM $MgCl_2$). Intracellular recordings were taken after 10 min of superfusion with 1x saline and then after 10 min of superfusion with 0.75x saline and were amplified with an AxoClamp 2B (Axon Instruments, Foster City, CA).

Electrophysiology data analysis

Recordings of CG bursting activity were analyzed for cycle period, burst duration, and duty cycle using custom Spike2 scripts to analyze bursting parameters. Bursting parameters were averaged over 10 bursts. Cycle period was defined as the time between the onset of two consecutive bursts, and duty cycle was defined as the ratio of burst duration normalized by the cycle period. For intracellular experiments, membrane potential (V_m) measurements were averaged over a period of 10 s. All statistical analyses were performed with GraphPad Prism 10.2.2 statistical software (GraphPad Software, Inc., Boston, MA). The Anderson-Darling test was used to check for normality (p>0.05). For normally distributed physiology data, comparisons of two groups were done using parametric paired t-tests (α=0.05). When comparing three paired

groups with non-normal distributions, a Wilcoxon signed-rank test was used in conjunction with a Bonferroni correction (α=0.0167). Comparisons of three independent groups with non-normal distributions were made with the Kruskal-Wallis test and the Dunn's multiple comparisons post-hoc test. Equality of variances was assessed with Levene's tests; in cases where more than two comparisons were made, alpha values were Bonferroni corrected. The ROUT method was used to identify and eliminate outliers.

Tissue collection

Cell harvesting was performed as previously described (Northcutt et al., 2019; Viteri & Schulz, 2023). Briefly, after experiments were completed, a petroleum jelly well was built around the CG. Saline inside the well was removed and replaced with nuclease-free protease (10 proteolytic units dissolved in saline; Sigma – 537088, St. Louis, MO) to digest connective tissue (15 min incubation). The well was then washed with three volumes of fresh saline to halt enzymatic activity. A gradual ice-cold ethylene glycol (EG) substitution (70% EG and 30% lobster saline) of the saline in the petroleum jelly well was performed over a period of 15 min. The lobster saline used for the EG solution matched the experimental condition. The saline outside the well was then replaced with distilled water, and the dish was frozen at –20°C for 1 h.

The large cells were collected using fine handheld forceps. To collect the small cells, the section of nerve just posterior to LC5 was clipped out. It should be noted that the section of nerve containing the small cells will also undoubtably contain neurite/axon projections, however, the small cells are too small to identify without fixing the tissue first. A section of axon containing no cell bodies (approximately equivalent in length to the small cell tissue) was collected from one of the anterolateral nerves of the CG. Tissue was placed in 400 µL RNA lysis

buffer (Zymo Research, Irvine, CA), flash-frozen in dry ice, and stored at –80°C until RNA extraction.

cDNA synthesis and pre-amplification of cDNA targets

RNA isolation and cDNA synthesis were performed as previously described (Northcutt et al., 2019). Briefly, total RNA was purified and isolated from individual neurons or tissues using the Quick-RNA MicroPrep kit (Zymo Research, Irvine, CA) according to manufacturer instructions. RNA samples were reverse transcribed using random hexamer and oligo(dT) primers (qScript cDNA Supermix; QuantaBio, Beverly, MA) in a reaction volume of 20 µL.

Eight microliters of cDNA was pre-amplified using SsoAdvanced PreAmp Supermix (Bio-Rad Laboratories, Inc., Hercules, CA) according to manufacturer instructions (24 µL reaction volume). The reactions were primed with a pool of target-specific primers to enrich genes of interest in subsequent RT-qPCR reactions. The preamplification cycling conditions were as follows: 95°C for 3 min; 14 cycles of 95°C for 15 s and 58°C for 4 min. Pre-amplified samples were then diluted with 76 µL of nuclease-free water to bring samples to a total volume of 100 µL.

Quantitative reverse transcription polymerase chain reaction (RT-qPCR)

Multiplex primer and probe sequences targeting the following six *H. americanus* genes were designed and validated (Table 1): voltage-gated delayed-rectifying K+ channel or Kv3 (*shaw1*), inward-rectifying K+ channel (*IRK*), L-type high-voltage-activated Ca^{2+} channel (*CaV1*), voltage-gated fast Na+ channel (*NaV*), hyperpolarization-activated inward current (*HCN*/*IH*), and sodium-potassium pump (Na^{+}-K^{+}*ATPase*). Primer sets and the associated probe sequence for each target gene are listed in Table 2. Probe fluorophore/quencher pairs used in this study were FAM-BHQ1 and CAL Fluor Gold 540-BHQ1.

Preamplified template (8 µL) was used to make a 32-µL reaction supermix, which included the following: 1) 6.4 µL of iTaq Universal Probes Supermix (Bio-Rad Laboratories, Inc.), 2) 1.6 µL of 50 µmol primer mix (IDT Integrated DNA Technologies, Coralville, IA), and 3) 1 µL of 10 µmol dual-labeled BHQ probe (LGC Biosearch Technologies, Petaluma, CA). This supermix was subdivided into 3 x 10 µL triplicates so that, for each qPCR reaction, a volume of 10 µL was loaded into a single well on a 96-well plate. The final primer concentration for each multiplex qPCR reaction was 2.5 µM, and the final concentration for each probe was 0.3125 µM. The CFX96 Touch Real-Time PCR Detection System (Bio-Rad) was used with the following cycling conditions: 95°C for 30 s; 40 cycles of 95°C for 5 s and 60°C for 30 s.

The sodium-potasium (Na^+-K^+) pump was assayed separately using SsoAdvanced Universal SYBR® Green Supermix (Bio-Rad Laboratories, Inc.) per manufacturer's instructions, with a 32 µL-reaction supermix consisting of: 1) 5 µL preamplified template, 2) SYBR® Green Supermix (16 µL), and 3) 8 µL of 20 µmol primer mix. The following PCR program was used: 98°C for 30 s; 40 cycles of 95°C for 15 s and 60°C for 30 s. Fluorescence measurements were acquired at the end of each cycle.

RT-qPCR data analysis

RT-qPCR data were processed using a modified $2^{-\Delta Cq}$ method in which the average quantification cycle (C_q) value for each target gene in the 1x or 0.75x condition was normalized to an arbitrary control value which represented the average C_q of all large cells in the 1x condition for the corresponding target gene. The result of this calculation (ΔCq) was then presented as $2^{-\Delta Cq}$ to represent relative mRNA expression. Processed data were plotted in Prism 10.2.2 (GraphPad Software, Inc.), with bars representing the median and error bars representing interquartile range. A Shapiro–Wilk test for normality was run to determine whether residuals for

each distribution were normally distributed ($P>0.05$). Relative mRNA expression distributions were compared across experimental groups using the Kolmogorov-Smirnov test, and the Mann-Whitney *U* test was used to compare mean ranks ($p<0.05$). Fisher's exact test was used to compare binomial proportions. Pairwise correlation relationships between any two channel mRNAs were tested using Spearman R values. Comparisons of slopes between two regressions were made with Prism's correlation analysis. Following previous work (Schulz et al., 2007), correlations were considered "strong" if the Spearman value was greater than 0.6 with a p value < 0.05.

RESULTS

Cardiac ganglion motor output was robust to long-term salinity perturbation

In order to study adaptive transcriptional changes in response to long-term salinity perturbation at the single cell level, I first determined whether the isolated cardiac ganglion (CG) neural circuit would reliably maintain its rhythmic motor output after 24 h exposure to two altered saline concentrations: 0.75x and 1.5x saline. 100% of CG preparations produced fictive rhythmic bursts of action potentials that would be consistent with driving heart contraction after 24 h in each saline condition. This is in line with other unpublished observations demonstrating that the lobster isolated CG continues to produce patterned neural activity when exposed briefly to salinity concentrations ranging from 0.5x–2x.

To determine if the CG neurons would adapt to a new physiological baseline of activity by simply being removed from the animal and any endogenous modulation that it receives *in vivo*, I also exposed the CG to 1x physiological saline for a period of 24 h as a time point control (Figure 3). While CG motor output was stable, the rhythm of the CGs slowed after 24 h in 1x saline, as indicated by a 78.60% increase in cycle period and 75.56% increase in burst duration (Figure 3B, C; paired *t*-test, cycle period: p=0.0003, burst duration: p=0.0013, N=12). To understand whether these changes in bursting characteristics affected the rhythmicity of the circuit, I also assessed duty cycle, which is the ratio of burst duration normalized by the cycle period—a measure of rhythmicity. I did not observe a change in duty cycle, indicating that the rhythmicity was not changed, but instead the CG output simply slowed (Figure 3D). However, a change in the CG's pattern of activity after 24 h in physiological saline is to be expected, given previous findings that simply removing endogenous neuromodulation by isolating the nervous system from the animal results in differences in ion channel mRNA abundances and, therefore, in neural output (Viteri & Schulz, 2023).

Exposure to 0.75x saline for 24 h had variable effects on CG bursting characteristics (Figure 4). No appreciable changes in cycle period were observed after acute (10 min) or 24 h exposure to 0.75x saline (Figure 4B; Wilcoxon signed-rank test, baseline vs. acute: p=0.67, acute vs. 24 h: p=0.90, baseline vs. 24 h: p=0.50, α=0.0167, N=16), and there was homogeneity of variances between baseline (1x), acute 0.75x, and 24 h 0.75x saline exposure (Levene's test, baseline vs. acute: p=0.10, acute vs. 24 h: p=0.034, baseline vs. 24 h: p=0.61, α=0.0167). However, a 61.65% increase in burst duration was observed after acute (10 min) exposure to 0.75x saline (Figure 4C; Wilcoxon signed-rank test, p=0.0006, α=0.0167), and a Levene's test indicated unequal variances between these two groups (baseline vs. acute: p=0.0029, α=0.0167). There was no appreciable change in the burst duration from the acute to 24 h timepoint (Wilcoxon signed-rank test, p=0.38), and the variance was similar between these timepoints (Levene's test, p=0.21), suggesting that the change in burst duration in the acute condition is sustained after 24 h. While burst duration at 24 h was not different from baseline, the variance in burst duration did change between baseline and 24 h (Levene's test, p=0.0002, α=0.0167). The increase in burst duration observed between baseline and acute 0.75x exposure is consistent with a concurrent increase in duty cycle observed between these two time points (Figure 4D; Wilcoxon signed-rank test, p<0.0001). There was no difference in duty cycle between acute and 24 h or between baseline and 24 h, nor were there differences in variances across the three time points (Wilcoxon signed-rank test, Levene's test, p>0.05). These data suggest that when 0.75x saline does elicit a change in burst characteristics upon acute exposure, this change is not necessarily compensated for after 24 h (i.e., burst characteristics do not consistently return to baseline values).

Similar trends were observed upon exposure to the more concentrated saline solution, 1.5x (Figure 5). While cycle period did not change from baseline with acute exposure to 1.5x saline, after a 24 h, I observed a 98.28% increase compared to the acute response, suggesting that bursting characteristics continue to change with long-term altered saline exposure (Figure 5B; Wilcoxon signed-rank test, p=0.0017, α=0.0167, N=14). This is reflected by the 122.42% increase in cycle period between baseline and 24 h of 1.5x exposure (Wilcoxon signed-rank test, p=0.004, α=0.0167, N=14). A Levene's test also indicated variance increased in response to a 24h exposure to 1.5x saline (p=0.0029, α=0.0167). Panels C and D of Figure 5 show that, although the burst duration did not consistently change with acute or 24 h exposure to 1.5x saline, the duty cycle decreased with acute exposure to 1.5x saline, indicating that the burst duration decreased compared to the relative inter-burst interval (not shown) within a given preparation, but no difference was observed between 24 h and acute or baseline (Wilcoxon signed-rank test; p=0.0067, α=0.0167).

Interestingly, the variability observed in the responses to altered salinity suggests that there may be multiple strategies to compensate for this perturbation. This variation is further demonstrated by comparing the burst characteristics of preparations at the 24 h timepoint in 1x and 0.75x saline (Figure 6). While there were no differences between these two conditions for cycle period, burst duration, or duty cycle (Mann-Whitney U test; Kolmogorov-Smirnov test; p>0.05), the variances between 1x 24h and 0.75x 24h groups were significantly different for burst duration and duty cycle, suggesting that 24 h exposure to 0.75x saline elicits variable responses in CG output (Levene's test, burst duration: p=0.0055, duty cycle: p=0.04, cycle period: p=0.08, N=12 for 1x 24 h preparations, N=16 for 0.75x 24 h preparations).

A lack of feedback and modulation that these neurons would typically receive *in vivo* may contribute to this variability in responses after 24 h, given that neuromodulation is known to be one of the mechanisms that constrains circuit output and regulates the correlated expression of ion channels (Temporal et al., 2012; Schneider et al., 2022; Viteri & Schulz, 2023). However, variation in response to 24 h exposure to altered salinity indicates that either individual neurons, or the circuit as a whole, is attempting to compensate for this perturbation.

Lack of perfect compensation after 24 h in altered saline suggests altered activity state

To better understand the variability of responses to 24 h of altered salinity exposure, I normalized the 24 h physiology data to the corresponding acute timepoint, which represents the extent to which bursting parameters continue to change after acute exposure (Figure 7). This transformation reveals that the system is not perfectly compensated after 24 h in altered salinity, and, instead, a different functional activity state is likely established at this timepoint. Interestingly, for both cycle period and burst duration, the 0.75x group clustered around zero (the acute timepoint baseline) whereas CG preparations exposed to 1x and 1.5x for 24 h continued to vary, suggesting that of the three salinity conditions, the system may be better compensated in 0.75x saline (Figure 7A, B).

A Kruskal-Wallis test indicated a significant difference in cycle period among the three salinity conditions ($H(2)=12.86$, $p=0.0018$). Variation from the acute timepoint was significantly lower in the 0.75x condition compared to 1x and 1.5x groups (Dunn's post-hoc test, 0.75x vs. 1x: $N_1=16$, $N_2=12$, $p=0.0159$; 0.75x vs. 1.5x: $N_1=16$, $N_2=14$, $p=0.0037$; 1x vs. 1.5x: $N_1=12$, $N_2=14$, $p\sim1$). A similar trend was observed for burst duration (Kruskal-Wallis test, $H(2)=10.19$, $p=0.0061$), where variation from the acute timepoint was significantly lower for 0.75x but was similar between 1x and 1.5x groups (Dunn's post-hoc test, 0.75x vs. 1x: $N_1=16$, $N_2=12$,

p=0.0084; 0.75x vs. 1.5x: N_1=16, N_2=14, p=0.0580; 1x vs. 1.5x: N_1=12, N_2=14, p~1). These results indicate that, after 24 h in 0.75x saline, bursting characteristics stabilize at some set point, but this does not necessarily occur in 1x or 1.5x saline.

While changes in cycle period and burst duration differed among the saline conditions after 24 h, changes in duty cycle were similar across the three groups, suggesting that rhythmicity is largely preserved in each salinity (Figure 7C; Kruskal-Wallis test, H(2)=1.611, p=0.4468).

The membrane hyperpolarized in response to 0.75x saline

To better understand the physiological response to altered saline, we performed sharp electrode intracellular recordings to assess whether acute (10 min) exposure to 0.75x saline alters the resting membrane potential of one of the large cells of the CG (Figure 8). In this experiment, I observed that, after just 10 min of exposure to 0.75x saline, the mean resting membrane potential was hyperpolarized to the baseline membrane potential (1x baseline: V_m= -54.5 mV; 0.75x saline: V_m= -61.1 mV). This hyperpolarization was expected because reducing the concentration of all extracellular ions alters the driving force on each of the ionic currents underlying the cell's activity, including potassium current. Because K^+ ions dictate resting membrane potential, reducing extracellular K^+ is expected to increase the driving force on K^+ to leave the cell, hyperpolarizing the membrane. A shift in the resting membrane potential also shifts the activation/inactivation kinetics for ion channels, resulting in a higher probability that these channels—namely, those carrying calcium-dependent current—will be de-inactivated/inactivated. We should also expect this hyperpolarized resting membrane potential to affect the hyperpolarization-activated inward current (I_h).

Relative mRNA abundances of six target genes did not differ between motor neuron subtypes with 0.75x saline

While I did not observe consistent changes in CG physiological output in response to salinity perturbation, due to ion channel degeneracy and coordinated shifts in channel correlations, it is possible that neurons are cryptically adjusting channel densities without appreciatively altering their output. Similarly, a lack of perfect adaptation to these perturbations over 24 h suggests that any compensation at the level of channel mRNA abundances is not perfect, if indeed happening at all. To address this question, I isolated individual motor neurons (large cells, LC) and premotor neurons (small cells, SC), as well as a section of axon from an anterolateral nerve in CG preparations that had been exposed to either 1x saline or 0.75x saline for 24 h. I then quantified relative mRNA abundances of five ion channel genes and one ion pump gene (Table 1) in each of these samples via RT-qPCR (see Methods). When comparing each motor neuron type (LC 1–5; N=8-10 for each LC) in the 1x control group to the corresponding group in 0.75x, I found that, on the whole, mRNA abundances in large cells do not change in a cell type-specific way with 0.75x saline. I found that relative *shaw1* (Kv3) mRNA abundances varied with 0.75x exposure in LC4 (Figure 11; KS test, p<0.05; Mann-Whitney U=14, N_1=N_2=9, p<0.05), and relative Na_V mRNA abundances varied with 0.75x exposure in LC3 (Figures 9 & 10; KS test, p<0.01; Mann-Whitney U=3, N_1=N_2=7, p<0.01). This change in Na_V mRNA abundance, however, may be due to three outliers in the 1x control group representing three individual neurons which may have had small pieces of axon attached when originally pulled from the ganglion, as higher Na_V mRNA expression is expected in the axon than in the somatic compartment. For both of these genes, no changes in mRNA abundances

were observed between 1x and 0.75x for any of the other motor neuron (LC) subtypes (KS test, $p>0.05$).

For each of the other gene targets (*CaV1*, Figure 11; *IRK*, Figure 12; *HCN/IH*, Figure 13; and *Na^+/K^+-ATPase*, Figure 14), relative mRNA abundances did not change with 0.75x saline in any of the large cells (KS test, $p>0.05$).

Notably, I did not observe differences in expression for any of the target mRNAs across the five motor neuron subtypes, indicating that large cells 1–5 likely express each of these mRNAs identically (Figures 9–14).

CaV1, IRK, and Na^+/K^+-ATPase mRNA abundances differed with 0.75x saline in total motor neuron population

Because there were no differences in relative mRNA abundances for each target gene across the five large cells, I pooled all LC samples together to determine the effect of 24 h exposure to 0.75x saline on the total large cell population (Figure 15; 1x saline: N=31-49; 0.75x saline: N=41-44). Whereas no differences in *CaV1*, *IRK*, and *Na^+/K^+-ATPase* mRNAs were found when comparing the large cells individually, pooling all larges cells together revealed a significant increase in mRNA abundances with 0.75x saline for each of these target mRNAs. For *CaV1*, exposure to 0.75x saline resulted in an approximately twofold increase in the median $2^{-\Delta Cq}$ value from the 1x condition and 0.75x groups (median $2^{-\Delta Cq}$ values were 0.926 for 1x and 1.57 for 0.75x; Hodges-Lehmann estimate of difference: 0.586). The rank sums in the two groups also differed significantly (Mann-Whitney U=689, N_1=45, N_2=43, $p<0.05$), as did their distributions (KS test; p=0.05). Similarly, for *IRK* (K_{ir}), the median $2^{-\Delta Cq}$ value increased fivefold with 0.75x saline from 0.262 for 1x to 1.26 (Hodges-Lehmann estimator: 0.404), and the rank sums in the two groups differed significantly (Mann-Whitney U=659, $N_1 = N_2 = 43$, $P<0.05$). For *Na^+/K^+-*

ATPase, the median $2^{-\Delta Cq}$ value increased approximately threefold with 0.75x, from 2.61 in the 1x condition to 7.34 (Hodges-Lehmann estimator: 2.30; Mann-Whitney U=765, N_1=46, N_2 =44, p<0.05). These results suggest that motor neurons upregulate their expression of three of the six genes tested in this study (*CaV1*, *IRK*, and *Na$^+$/K$^+$-ATPase*)—two of which are inward currents—in response to reduced extracellular ionic concentration, indicating that large cells may, in fact, be able to adjust their channel densities in response to external perturbations (Figure 15A, D, F).

CaV1 and HCN/IH mRNA abundances differed with 0.75x saline in premotor neurons

Because intrinsic activity in the four pacemaker small cells (premotor neurons) is responsible for driving bursting activity via excitatory electrochemical input to the motor neurons, it was important to measure their relative mRNA abundances in response to salinity perturbation as well. To do this, I collected small cell (SC) samples by clipping out the section of neurite just posterior to LC5 (see Figure 2), which should contain all four small cells. As a result, relative mRNA expression in these tissues was higher than that seen in individual LC samples, and thus, I plotted their mRNA abundances separately. When comparing the relative mRNA abundances between small cells in 1x and 0.75x saline, I found no differences for *shaw1*, *NaV*, *IRK*, or *Na$^+$/K$^+$-ATPase* mRNAs (KS test, Mann-Whitney *U* test, p>0.05; Figures 18–21). However, relative abundances for *HCN/IH* and *CaV1* mRNAs did differ significantly with 0.75x saline in the small cells (Figures 22–23). For *HCN/IH*, the median $2^{-\Delta Cq}$ value increased from 37.81 in 1x saline to 118.2 (an approximately threefold increase) in 0.75x saline (Hodges-Lehmann estimator: 71.8), and the rank sums in the two groups differed significantly (Mann-Whitney U=13, $N_1 = N_2 = 10$, p<0.01). Distributions of the two groups differed as well (KS test, p=0.05). An increase in *HCN/IH* mRNA abundance is in line with the observation that the

membrane hyperpolarizes in response to reduced salinity (Figure 10), as increased *HCN* channel production would likely increase the excitability of the neuron. As seen in the large cells, relative *CaV1* mRNA abundance increased about twofold with 0.75x saline in the small cells, with the median $2^{-\Delta Cq}$ value increasing from 12.48 in 1x saline to 39.37 (Hodges-Lehmann estimator: 13:55), and the rank sums differed significantly (Mann-Whitney U=16, N_1 = 10, N_2 = 9, p<0.05). Distributions of the two groups did not differ (KS test, p=0.0660).

NaV mRNA abundances change with 0.75x saline in the cardiac ganglion

I observed an interesting phenomenon when assaying CG tissue for *NaV* mRNA wherein, in about 36.17% of the total large cell population exposed to 1x saline (N=47 large cells total), *NaV* transcript was not expressed at a high level and was undetectable in the sample. This low level of expression in LCs was expected, as work demonstrating that driver potentials in the lobster CG are tetrodotoxin (TTX)-insensitive suggests that NaV channels should not be highly expressed in the somatic compartment, given that these channels are sensitive to TTX (Tazaki & Cooke, 1983). Previous molecular characterization of *NaV* expression in the stomatogastric ganglion in *Cancer borealis* confirmed that *NaV* expression is compartment-specific, with *NaV* mRNA most abundant in the axon (Ransdell et al., 2010). Indeed, in the samples in which *NaV* mRNA was detected, the median $2^{-\Delta Cq}$ value was low (1x saline: 0.0004180; 0.75x saline: 0.0001950). Interestingly, however, among the total LC population in the 0.75x group, the percentage of undetectable transcript levels decreased to 6.98% (N=43). This suggests that, despite not observing appreciable changes in mean mRNA abundances, whether or not *NaV* mRNA is expressed at detectable levels is impacted by 0.75x saline exposure, and exposure to 0.75x saline increases the likelihood that *NaV* mRNA will be expressed at detectable levels.

The opposite trend was true for axon samples, where *NaV* mRNA was detected in 100% of samples exposed to 1x saline (*N*=10), but in the 0.75x group, only 1 of 10 samples (1%) expressed *NaV* transcript. As a result, relative mRNA abundance could not be quantified for the axon samples. The small cells did not appear to be affected as dramatically, as 50% of SC samples did not express *NaV* at detectable levels in the 1x condition, and 40% of samples did not express *NaV* in the 0.75x group. These observations suggests that 0.75x saline exposure modulates *NaV* expression patterns in a cell type-specific way in the CG.

To better represent *NaV* mRNA expression patterns, I created a binary scoring system in which individual samples were assigned a score of 1 or 0 based on whether detectable levels of *NaV* mRNA were present or not, respectively. Figure 22A shows the mean score for each cell type in 1x and 0.75x saline. Using this binomial scoring system, I observed that *NaV* mRNA was significantly less likely to be present in the 0.75x condition for the axon samples compared to control 1x saline (Fisher's exact test, p=0.0001). *NaV* was the only gene for which I saw changes in expression in the axon with 0.75x saline, which makes sense, given that it is the only gene I tested whose expression is localized primarily to this tissue.

While the probability of observing *NaV* transcript in individual large cells did not change with 0.75x saline, measuring this probability in the total large cell population revealed a significant increase in the likelihood of observing *NaV* mRNA with 24 h exposure to 0.75x saline (Figure 22B). A simultaneous decrease in *NaV* mRNA presence in the axon and an increase in its presence in the motor neurons suggests that perhaps altered salinity affects mRNA trafficking such that *NaV* mRNAs in the axon are directed toward somatic compartments.

Correlated channel mRNA relationships in motor neurons were lost with salinity perturbation

Previous work has suggested that pairwise channel mRNA relationships, rather than abundances, may in fact be a better indicator of cell state or identity (Viteri & Schulz, 2023). Therefore, I was interested in whether salinity perturbation shifts mRNA relationships which would indicate altered cellular function. Of the six targets tested in this study, four significant channel relationships were identified in the large cell population: *shaw1* and *CaV1; HCN/IH* and *CaV1; HCN* and *IRK*; and *NaV* and *HCN/IH* (Figure 23). In each of these cases, a significant positive relationship was observed in the 1x condition (Spearman value > 0.6, $p<0.05$), but this correlation was lost in the 0.75x condition (Spearman value < 0.6, $p>0.05$).

These same channel mRNA relationships were tested in the small cells, however, only *HCN* and *CaV1* were strongly correlated in 1x saline (Figure 24B). As was the case in the large cells, this relationship was lost in 0.75x saline.

Because coordinated ion channel mRNA relationships are thought to underlie the maintenance of stable neural output, the loss of these correlated channel relationships with 0.75x saline suggests that this perturbation disrupts stable activity relationships which must be compensated for via activity-dependent feedback mechanisms (Zhao & Golowasch, 2012).

DISCUSSION

The ability to withstand global perturbations to the extracellular environment is an essential feature of central pattern generator neural networks, like the cardiac ganglion (CG) in *Homarus americanus*. How behavior and circuit performance can be maintained despite environmental challenges, such as altered salinity, is a fascinating question that has not been well-studied at the molecular level. The present study aims to address whether individual neurons of the cardiac ganglion sense and compensate for long-term changes in extracellular ionic concentration by adjusting their ion channel mRNA abundances to achieve circuit stability in response to environmental challenge.

The results of this study indicated that, indeed, the CG is robust to salinity perturbations in both the short-term and over a period of 24 h, as the rhythmicity of the circuit was preserved with 24 h exposure to 0.75x or 1.5x saline. These changes in saline concentrations are much more dramatic than the nervous system would typically experience *in vivo*, and thus I expected to observe changes in motor output in response to this perturbation. On the whole, acute (10 min) exposure to altered saline elicited significant changes in bursting characteristics; however, after 24 h of exposure to this perturbation, the system was not perfectly compensated, as I observed variation in bursting characteristics at this timepoint, suggesting that preparations do not necessarily return to a baseline or target activity but, rather, stabilize at a new homeostatic "set point." This is in line with conceptual models of neuronal homeostasis suggesting that target activity is not fixed in time and, therefore, imperfect compensation can be tolerated by the system (O'Leary et al., 2014). The question, then, is whether neurons are able to sense this change in activity and adjust their channel densities accordingly.

An important contribution of this study is that we show that neurons of the CG alter their ion channel mRNA abundances in response to long-term salinity perturbation and that the two

CG cell types (motor neurons and premotor neurons) do so differently. Because we found that the large motor neurons of the CG express ion channels identically, when pooled together, the total large cell population upregulated expression of two inward currents—*CaV1* (Ca_V) and *IRK* (K_{ir})—as well as *Na+/K+-ATPase* (sodium-potassium pump) in response to 0.75x saline. Because sharp electrode intracellular recordings indicated that brief exposure to 0.75x saline hyperpolarizes the resting membrane potential compared to 1x saline (Figure 10), which, in turn, increases the probability that ion channels will be deinactivated/inactivated, we hypothesized that membrane excitability may be enhanced in 0.75x saline. Upregulation of inward current ion channel mRNAs whose protein products activate at depolarized potentials and contribute to cation influx into the cell, therefore, is not a surprising consequence of exposure to decreased extracellular ionic concentration.

Relative *CaV1* mRNA abundance also increased in the premotor neurons (small cells, SC) with 0.75x saline. Because *CaV1* mediates influx of Ca^{2+} into the cell in response to depolarizing potentials, upregulation of these channels supports the idea that extracellular calcium fluctuations may play a role in intracellular signaling and transcriptional regulation. However, no additional ion channel mRNAs that were significantly upregulated in large cells were also changed in small cells. This is in line with our understanding of the large cells and small cells as two distinct cell types, and therefore, we should expect their ion channel profiles to differ, reflecting their differing functional requirements. We did observe a significant upregulation of *HCN/IH* channel mRNAs in the small cells with 0.75x saline, which is congruent with physiological observations that the membrane hyperpolarizes when briefly exposed to a reduced saline concentration. These channels pass a nonselective cation (I_h) current and activate

at hyperpolarized membrane potentials, contributing to cell depolarization. Thus, it is possible that the cell senses its voltage and upregulates *HCN/IH* in response.

Expression patterns of the fast sodium channel mRNA (*NaV*) were changed in an unexpected manner with salinity perturbation. We did not expect *NaV* to be highly expressed in the somatic compartment because of physiological and molecular studies reporting low abundance in somata (Tazaki & Cooke, 1983; Ransdell et al., 2010). Indeed, we found that *NaV* transcript could not be detected by RT-qPCR in about a third of the large cells in 1x saline, suggesting this transcript was either absent or expressed at such low levels that it could not be amplified with 40 cycles of PCR. In the remaining cells in which *NaV* transcript was detected, its relative abundance was low in comparison to other genes. Conversely, as anticipated, we observed high expression the axon, where *NaV* mRNA is reported to be most abundant. However, this expression was dramatically reduced in 0.75x saline, such that transcript was detected in only one of ten axon samples, suggesting that, following salinity perturbation, *NaV* transcript is either not present or is expressed at very low levels. The reverse was true for large cells, where we saw that the incidence of undetectable levels of mRNA decreased from 36.17% to just 6.98% in 0.75x saline. This led us to develop a binomial scoring system to better characterize the expression patterns of *NaV* with salinity perturbation wherein samples with detectable transcript were assigned a value of '1,' and samples with undetected levels of mRNA were assigned a value of '0.' This allowed us to determine the probability of detecting *NaV* in a given sample, revealing that 0.75x saline exposure caused a significant increase in the probability of observing *NaV* transcript in the large cells and a concomitant decrease in its presence in the axon (Figure 22). This is an interesting finding, as it suggests that perhaps salinity perturbation elicits changes in mRNA trafficking and a reversal of the compartment-

specific localization of *NaV* while under physiological conditions. A reduction in *NaV* mRNA in the axon may mean a decrease in local translation of NaV channel proteins in the axon and the coordinated activation of *NaV* transcription in somata. Another theory that has not yet been studied in the CG is that mRNA levels are under the regulation of microRNAs that maintain ion channels, including NaV, in the proper proportion. If, for instance, miRNAs targeting NaV are downregulated in large cells in response to salinity perturbation, or are upregulated in the axon, this may explain the phenomenon we observe in the present study. While the mechanism behind this observation is unclear, these data suggest that differential regulation of *NaV* mRNA is a component of the adaptive response to salinity perturbation.

While we observed changes in mRNA abundance with salinity perturbation, it should be noted that these changes are relatively modest. One explanation for the relatively small changes in channel mRNAs that still give rise to maintenance of circuit function after perturbation is that ion channel kinetics are being altered by post-translational modifications like phosphorylation/de-phosphorylation that cannot be measured at the single-cell level. Another explanation may be that the CG receives feedback from the cardiac muscle, and therefore, it is possible that this feedback itself dynamically controls CG output in response to perturbations, and that this effect is underappreciated by studying the CG in isolation.

However, changes in correlated channel mRNA relationships with 0.75x salinity would suggest that these modest changes in mRNA abundance are sufficient to impact activity. It has been well-established that certain ion channels are co-regulated, and that their coordinated expression gives rise to particular activity states that can be maintained homeostatically or, if shifted or lost, may indicate altered activity states (O'Leary et al., 2013; Temporal et al., 2014). Because we tested six genes in this study, there were 64 possible pairwise relationships. Of these,

we found four pairs of ion channels with significantly correlated patterns of expression in control (1x 24 h) large cells: *shaw1* and *CaV1; HCN/IH* and *CaV1; HCN* and *IRK*; and *NaV* and *HCN/IH*. Strikingly, each of these correlations were lost with 24 h of 0.75x salinity perturbation (Figure 23). Loss of correlated channel relationships suggests that changes in extracellular ionic concentration disrupts stable channel correlations, potentially indicating the establishment of an altered activity or cell state with prolonged exposure to salinity perturbation. It is possible that new, previously-uncorrelated relationships may form with altered salinity if we were to assay additional genes.

Indeed, a large portion of the dataset for this study is missing. We would like to measure six additional mRNAs: *BKKCa* (large-conductance calcium-activated potassium channel), *SKKCa* (small-conductance calcium-activated potassium), *shaker* (voltage-gated A-type potassium, I_A), *shab* (voltage-gated delayed rectifier potassium or Kv2), *KCNK1* (two-pore domain leak potassium), and *NALCN* (non-selective sodium leak). Each of these are genes for which we have validated primer sets (Table 3), and which we expect will exhibit greater changes in expression in response to salinity perturbation. Future plans include assaying 1.5x samples for each of these genes as well—tissue samples for the 1.5x condition have been collected and prepared for RT-qPCR experiments. Adding these genes to our dataset will clarify the effect of salinity perturbations on gene expression in CG neurons and may allow us to develop a theory on the potential homeostatic mechanisms underlying circuit robustness to salinity. It also must be stated that relationship between mRNA levels and protein products is not necessarily linear—we cannot be sure that changes in mRNA abundances accurately reflect changes in ion channel densities. Because of this, it will be important to perform voltage clamp experiments using channel blockers to assess whether channel conductances change as we would expect based on

their mRNA abundances. Ultimately, understanding how neurons sense and adapt to changes in their extracellular environment will inform our understanding of homeostatic systems and why, for instance, the nervous system may not be able to compensate for loss of function in pathological contexts.

FIGURES & TABLES

Table 1. List of *H. americanus* genes measured by RT-qPCR in this study.

Gene name	Current/channel type
shaw1	Voltage-gated delayed rectifier potassium (I_{Kd})
IRK	Inward-rectifier potassium (I_{Kir})
CaV1	L-type high-voltage-activated calcium
NaV	Voltage-gated fast sodium *para* type
HCN/IH	Hyperpolarization-activated current (I_h)
Na^+/K^+-ATPase	Na^+/K^+-ATPase alpha subunit (sodium-potassium pump)

Table 2. Target primer and probe sequences for RT-qPCR experiments. Each box represents the genes that were assayed in a duplex or single-plex reaction.

Gene	Accession #	Forward/Reverse Primer 5′-3′ sequence	Probe 5′-3′ sequence
CaV1	KU702651.1	TCCAGGCAGGTTTGAGAACTTTG/GTCATCGTCACGCATTTCATCTAAG	CTGGACCTGAGCTGAAGCGTGC
shaw1	KU681443.1	CGAGCCAAACTTCCCAAGAAAC/GGACCGCGATTCATGTCATTG	AGTCCTGCCCGTGGAGCACGT
NaV	KU702653.1	GTCAGCACAAGGATCAGTCATC/CAGTGTCTGCTTGCTTCAGTTC	CTTTCCGGTGCCGAGTCCCAG
IRK	KU681439.1	TGTCCCGAGGCCATATTTGTC/TGCCGACCATAAATGCCTGTATC	TGCATCCAGAGCATCACAGGTGT
HCN/IH	KU712077.1	TGCGAGCTGAGACTTACTGTAAC/CCGTCGCATGAGCGGATAG	TCAGCCTCAGTGTGGAACATTTCAACA
Na^+/K^+-ATPase	AY140650.1	TCGTTCACCAGGGCATGAAG/GGAAGGCAGCCAGTGTAGTT	

Table 3. Validated primer sets for six additional gene targets.

Gene	Accession #	Forward/Reverse Primer 5′-3′ sequence
BKKCa	KU712072.1	TCGGTGAAGGTGGCAAGTATG / TGATGTGTCGCGGAATCTGTAG
SKKCa	KU712071.1	CAACACGCGGTTTGTTCTCAAG / AGTGTCCACGAGGCAATGATC
KCNK1	KU681450.1	TGTGGCCTTTGCCCTTATCTTC / GGCTTCGTCACGTCTTTCGT
shaker	KU702655.1	GTGGCCATCATCTCCGTCTTC / TGCCGTTGGTCGTGGTATT
shab	KU701656.1	GCCATGGGCGTGTTAGTCT / CCGCCCACCAGAAAGTCTC
NALCN	KU681445.1	TGGCACGAGAAGAGCTAGA / TCAAGCCAGTTGCGAATAGTC

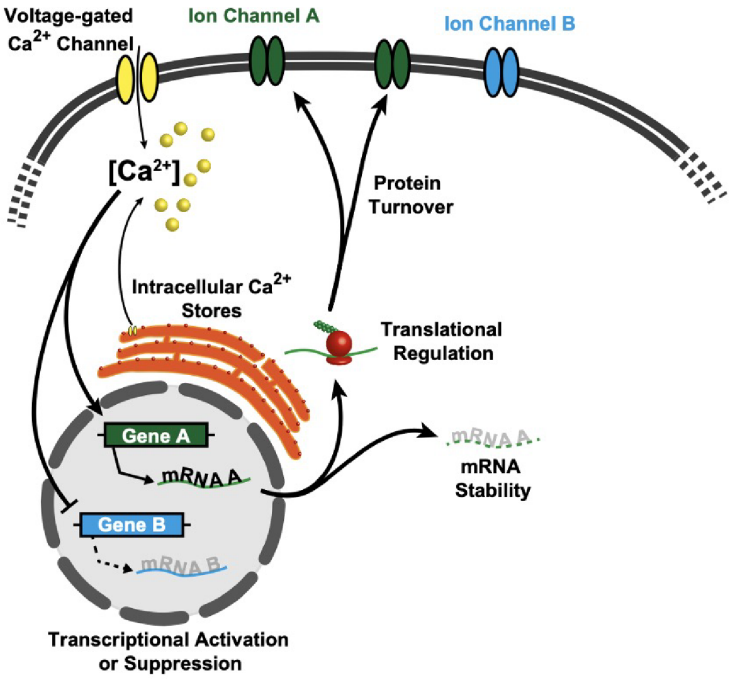

Figure 1. Proposed model of activity-dependent gene regulation mediated by intracellular calcium concentration. Adapted from Northcutt & Schulz, 2019.

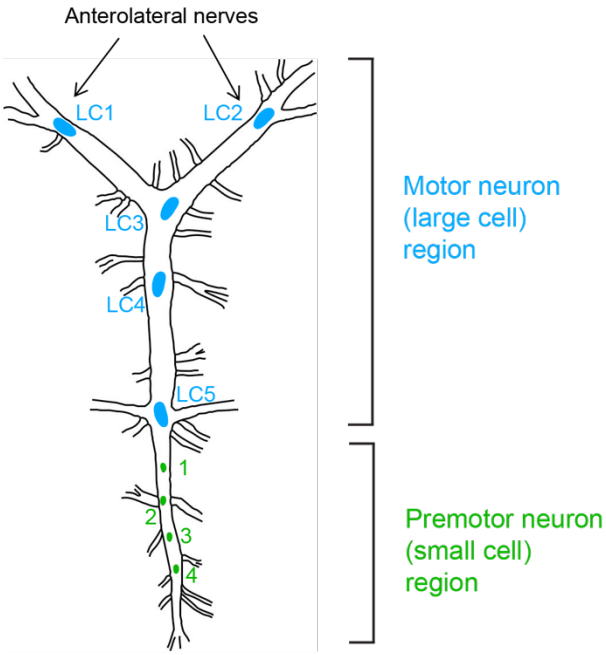

Figure 2. Schematic diagram of the isolated cardiac ganglion (CG) preparation. Five motor neurons (large cells, LC) and four premotor neurons (small cells, SC) are identified.

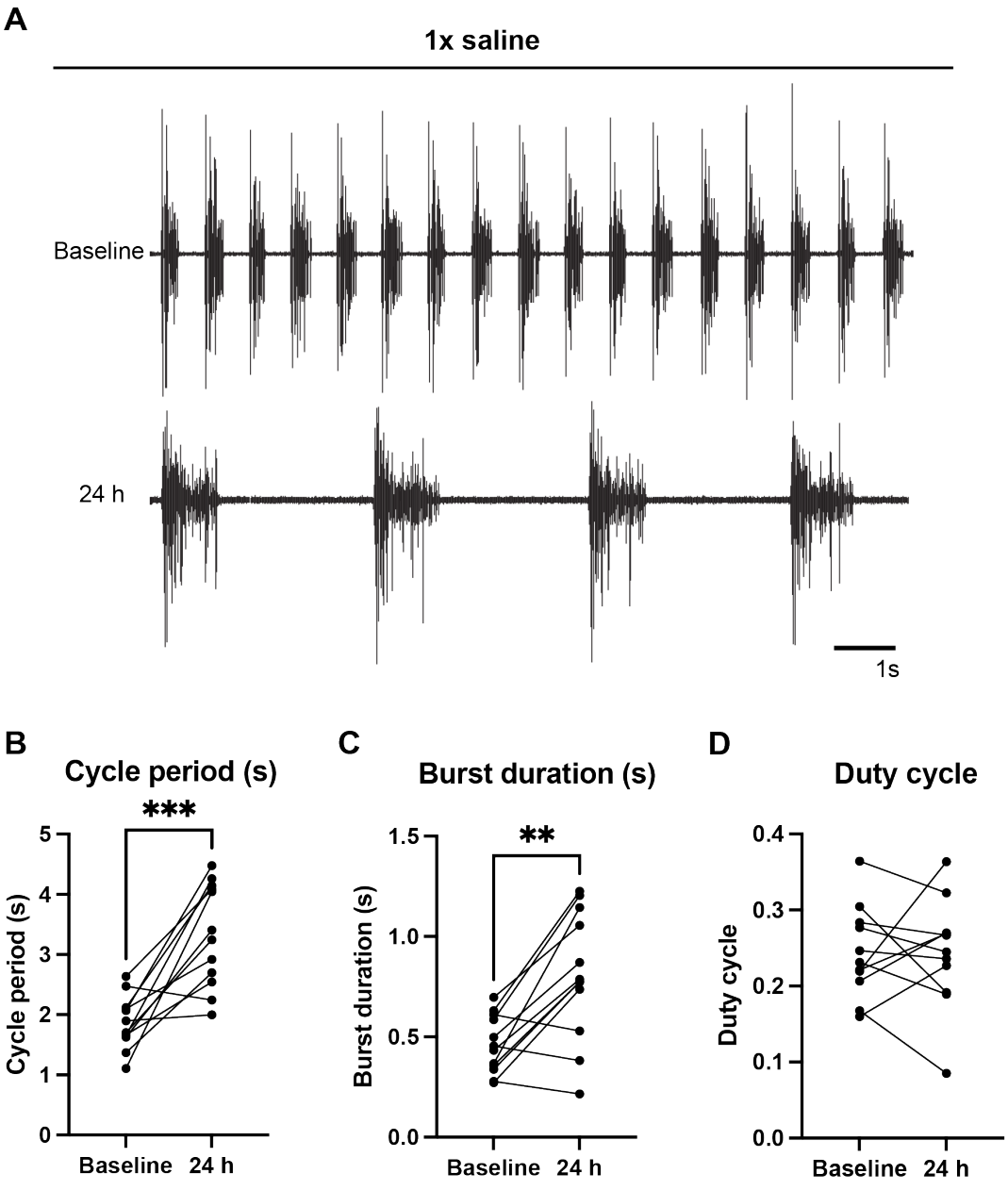

Figure 3. 24 h exposure to 1x *H. americanus* saline alters bursting characteristics of the isolated cardiac ganglion. (A) Representative trace of bursting activity in the CG at baseline and after 24 h in 1x physiological lobster saline. **(B)** Cycle period (time between onset of consecutive bursts) increased after 24 h in 1x saline (paired t-test, ***p<0.001, N=12). **(C)** Burst duration increased after 24 h in 1x saline (paired t-test,**p<0.01, N=12). **(D)** No change in duty cycle was observed between baseline and 24 h in 1x saline (Wilcoxon test, p>0.05, N=12). ROUT method was used to eliminate outliers.

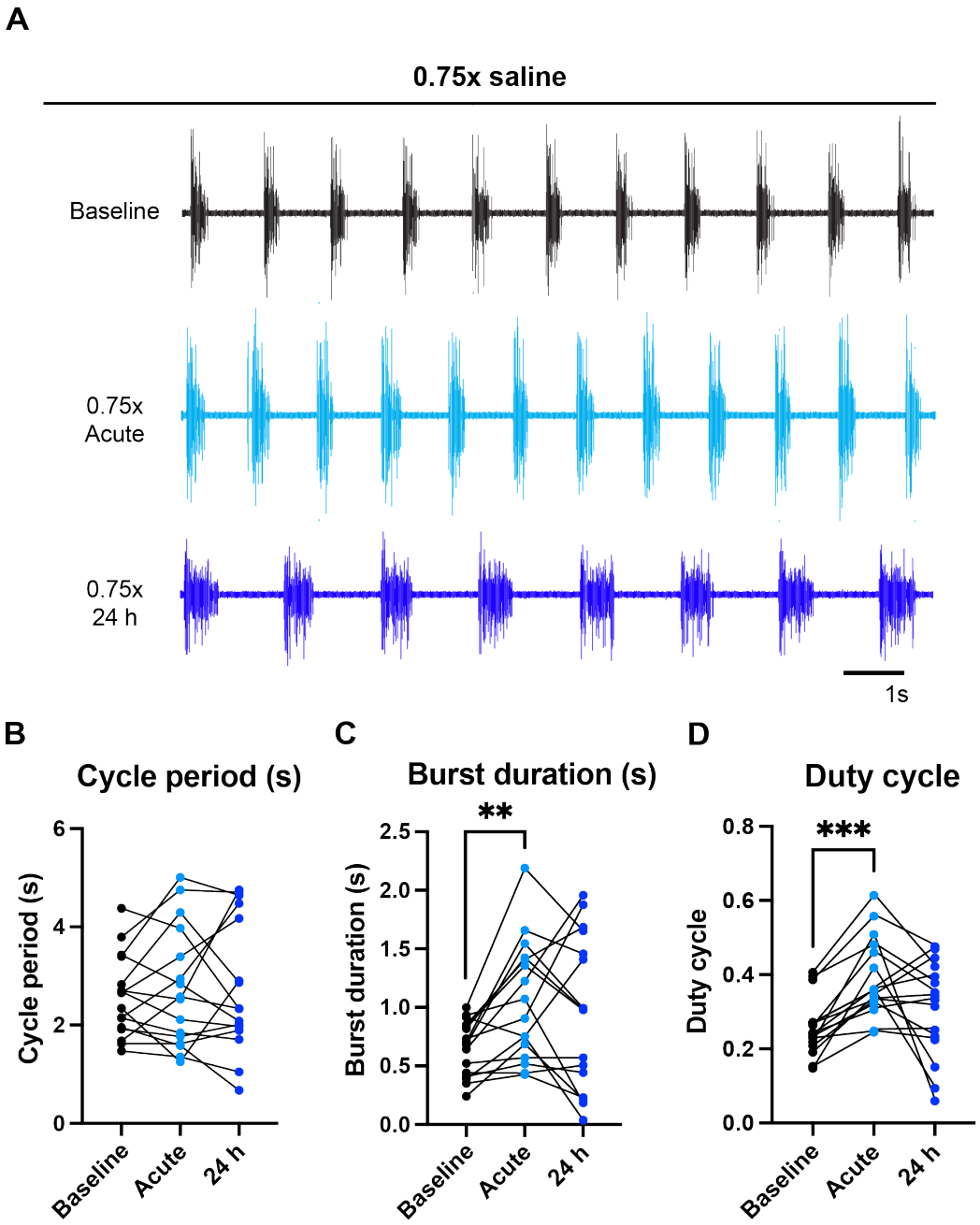

Figure 4. Effect of 24 h exposure to 0.75x *H. americanus* saline on burst characteristics of the isolated cardiac ganglion. (A) Representative trace of bursting activity in the CG at baseline, after 10 min in 0.75x saline, and after 24 h in 0.75x saline. **(B)** No change in cycle period was observed after acute (10 min) or 24 h exposure to 0.75x saline (Wilcoxon signed-rank test, $p>0.05$, $N=16$). There was homogeneity of variances between baseline, acute, and 24 h timepoints (Levene's test, $p>0.05$). **(C)** Burst duration increased with acute exposure to 0.75x saline, but no difference was observed after 24 h exposure to 0.75x saline compared to baseline or acute (Wilcoxon signed-rank test, $^{**}p<0.01$, $N=16$). There was unequal variances between baseline and acute and between baseline and 24 h (Levene's test, $p<0.01$). **(D)** Duty cycle increased with acute exposure to 0.75x saline, but no difference was observed between 24 h and acute or baseline (Wilcoxon signed-rank test, $^{***}p<0.001$). There was homogeneity of variances between each group (Levene's test, $p>0.05$).

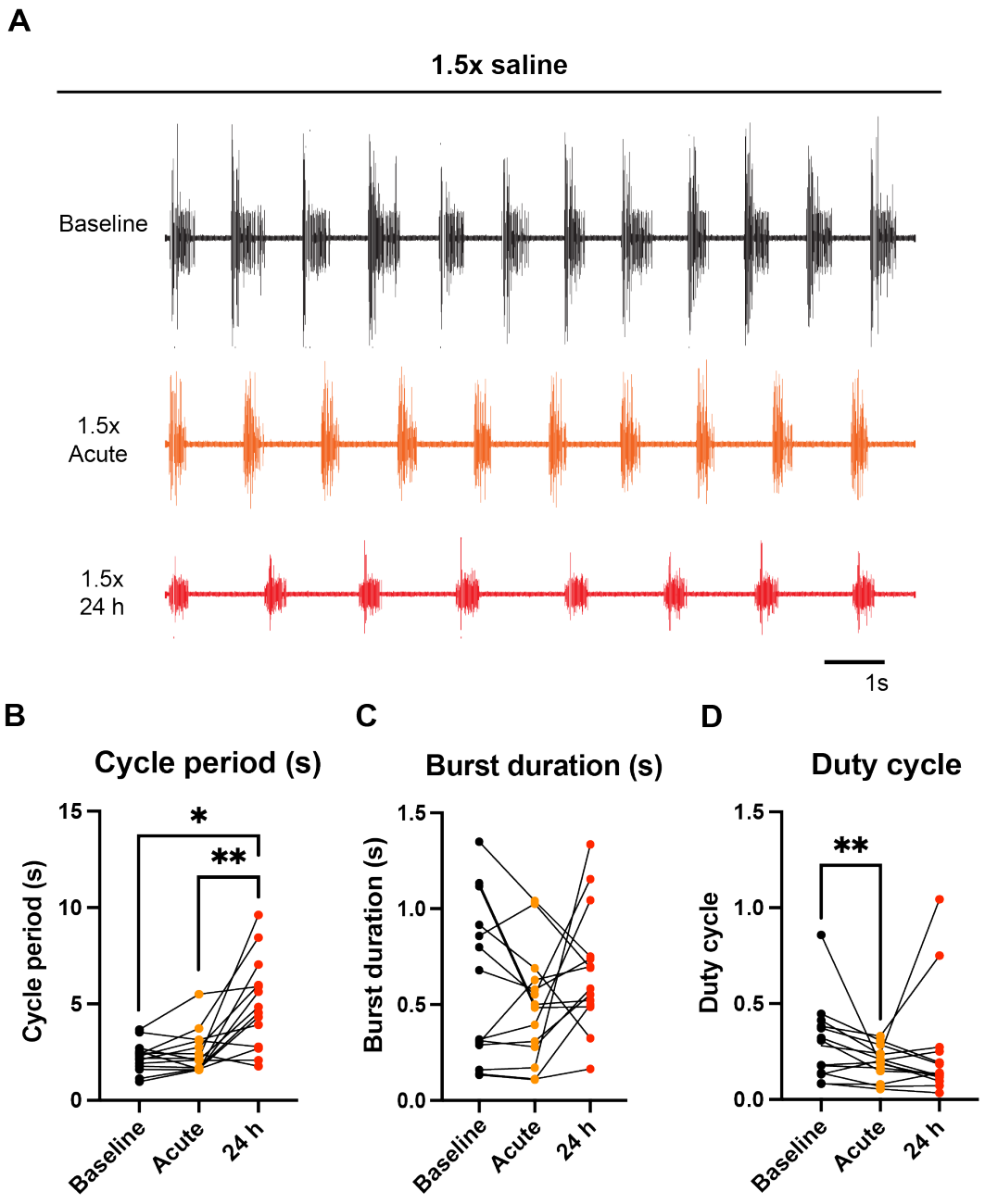

Figure 5. Effect of 24 h exposure to 1.5x *H. americanus* saline on burst characteristics of the isolated cardiac ganglion. (A) Representative trace of bursting activity in the CG at baseline, after 10 min in 1.5x saline, and after 24 h in 1.5x saline. **(B)** Cycle period was significantly greater after 24 h in 1.5x saline compared to baseline and increased between acute (10 min) and 24 h exposure (Wilcoxon signed-rank test, *p<0.05, **p<0.01, N=14). There was unequal variances between baseline and 24 h timepoints (Levene's test, p<0.01) but homogeneity of variances between baseline and acute and between acute and 24 h. **(C)** Burst duration did not change with acute or 24 h exposure to 1.5x saline (Wilcoxon signed-rank test, p>0.05, N=14). There was homogeneity of variances between baseline, acute, and 24 h timepoints (Levene's test, p>0.05). **(D)** Duty cycle decreased with acute exposure to 1.5x saline, but no difference was observed between 24 h and acute or baseline (Wilcoxon signed-rank test, p<0.05, N=12-14). There was homogeneity of variances between all groups (Levene's test, p>0.05). ROUT method was used to eliminate outliers.

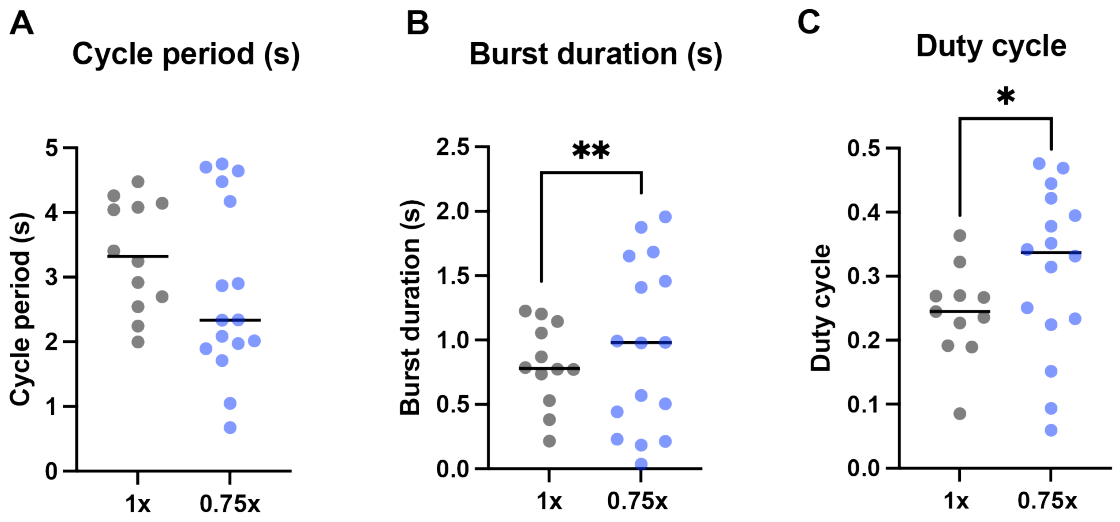

Figure 6. Changes in burst characteristics after 24 h in 0.75x saline compared to 24 h in 1x saline. Variances of burst duration and duty cycle differed after 24 h in 0.75x saline compared to 24 h in 1x saline (Levene's test, *p<0.05, **p<0.01, N=12-16). The median value and distribution did not change with 0.75x saline for any of the bursting parameters (Mann-Whitney U test, p>0.05; K-S test, p>0.05).

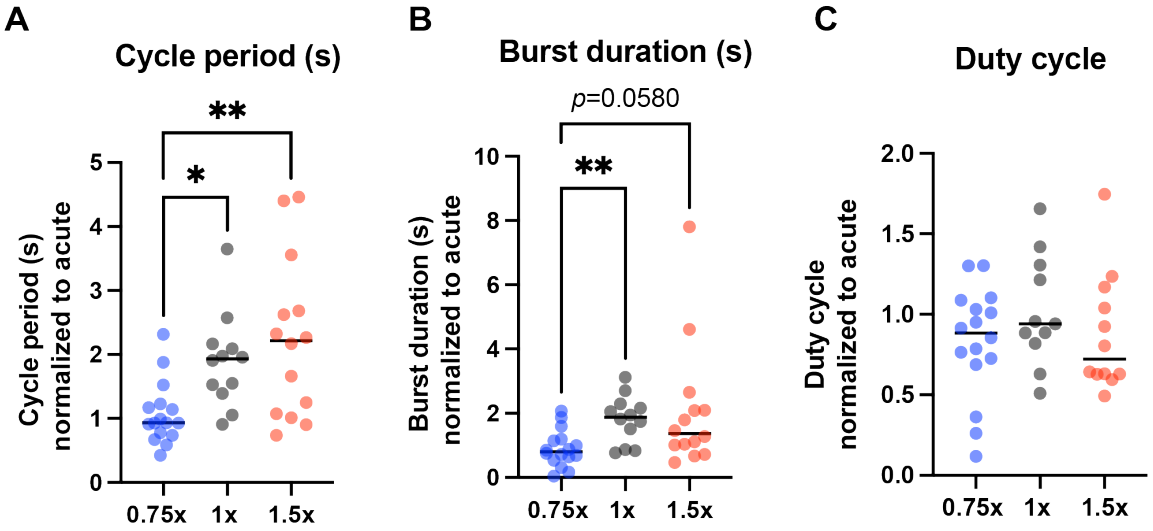

Figure 7. Changes in burst characteristics after 24 h normalized to acute timepoint. (A) For cycle period, there was a significant difference between the 0.75x and 1x groups and between the 0.75x and 1.5x groups, with a mean rank of 12.94 for 0.75x 24 h, 26.00 for 1x 24 h, and 27.43 for 1.5x 24 h normalized data (Kruskal-Wallis test, *p<0.05, **p<0.01, N=12-16). **(B)** For burst duration, there was a significant difference between the 0.75x and 1x groups (Kruskal-Wallis test, **p<0.01), and the difference between 0.75x and 1.5x groups had a p value of 0.0580 (N=12-14). The mean rank was 14.00 for the 0.75x 24 h normalized data, 28.00 for 1x 24h, and 24.50 for 1.5x 24 h. **(C)** There were no differences between groups for duty cycle (Kruskal-Wallis test, p>0.05, N=11-12).

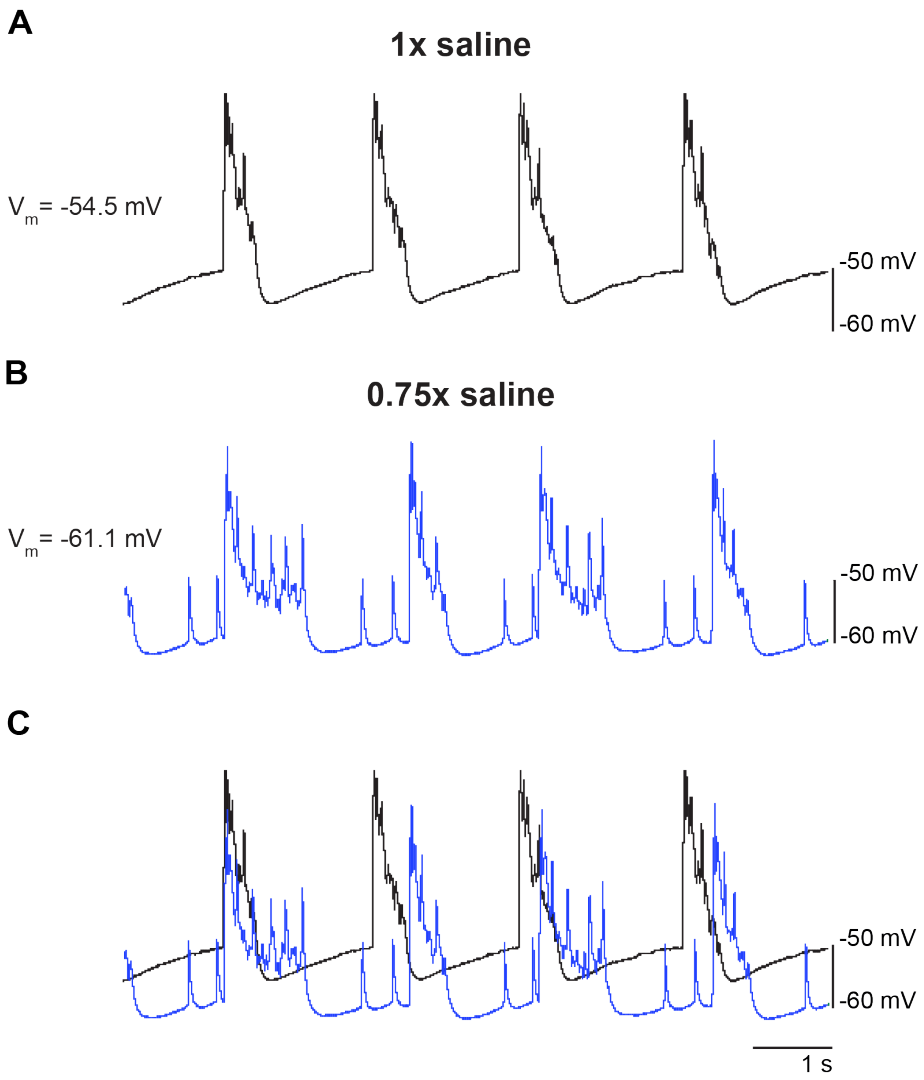

Figure 8. Resting membrane potential is hyperpolarized after 10 min in 0.75x saline compared to baseline in 1x saline. Example intracellular recording from large cell 2 in one isolated cardiac ganglion preparation. **(A)** Baseline membrane potential in 1x saline was -54.5 mV. **(B)** Membrane potential hyperpolarized from baseline (-61.1mV) with acute exposure to 0.75x saline. **(C)** Overlay of traces shown in panels A and B.

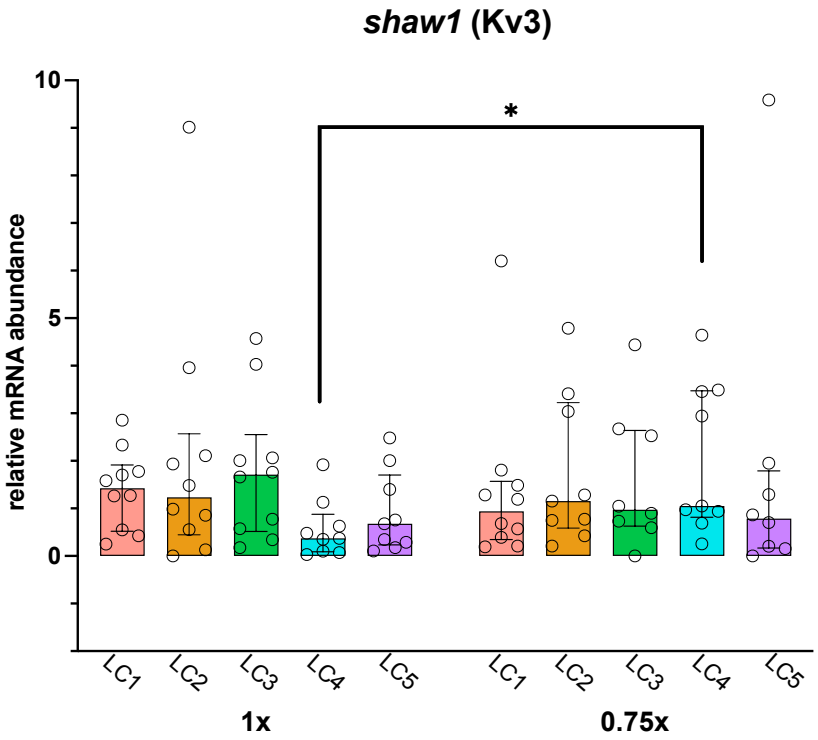

Figure 9. Effect of exposure to 0.75x saline for 24 h on the relative abundance of *shaw1* mRNA in large cells of the cardiac ganglion. Boxplots displaying relative mRNA abundance in large cells (LC) 1-5 after 24 h in 1x saline and 0.75x saline. Each circle represents an individual neuron (*N*=8-10). Relative mRNA abundance was uniform across each LC in the 1x 24h control condition. In LC4 (*N*=9), the distributions in 1x and 0.75x were significantly different (*p<0.05, Mann-Whitney *U* test). No changes were observed across 1x and 0.75x conditions in the other LCs. Bars represent the median value, and error bars represent interquartile range.

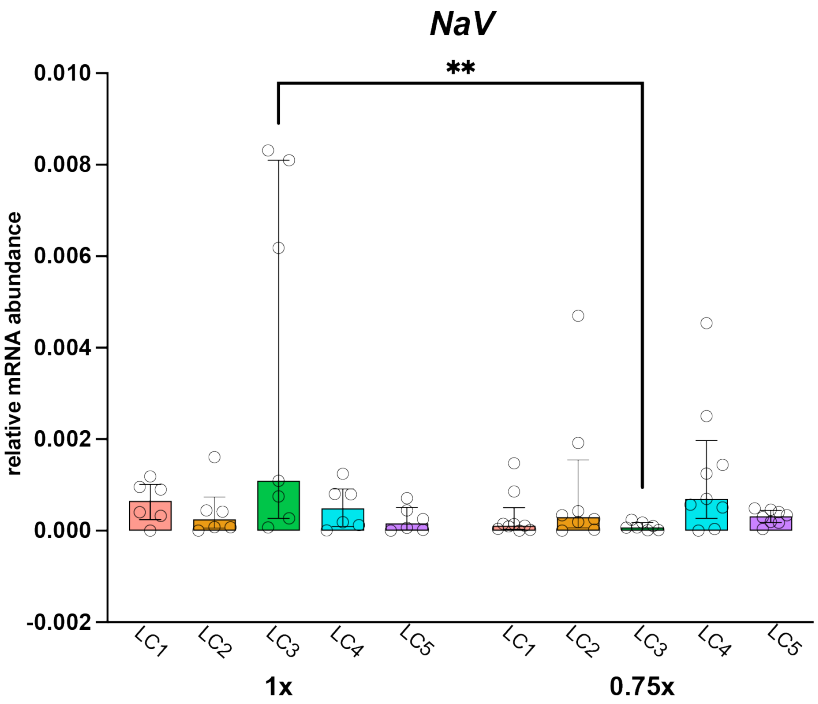

Figure 10. Effect of exposure to 0.75x saline for 24 h on the relative abundance of *NaV* mRNA in large cells of the cardiac ganglion. Boxplots displaying relative mRNA abundance in large cells (LC) 1-5 after 24 h in 1x saline and 0.75x saline. Each circle represents an individual neuron (*N*=8-10). Relative mRNA abundance was uniform across each LC in the 1x 24h control condition. In LC3 (*N*=7), the distributions in 1x and 0.75x were significantly different (***p*<0.01, Mann-Whitney *U* test). No changes were observed across 1x and 0.75x conditions in the other LCs. Bars represent the median value, and error bars represent interquartile range.

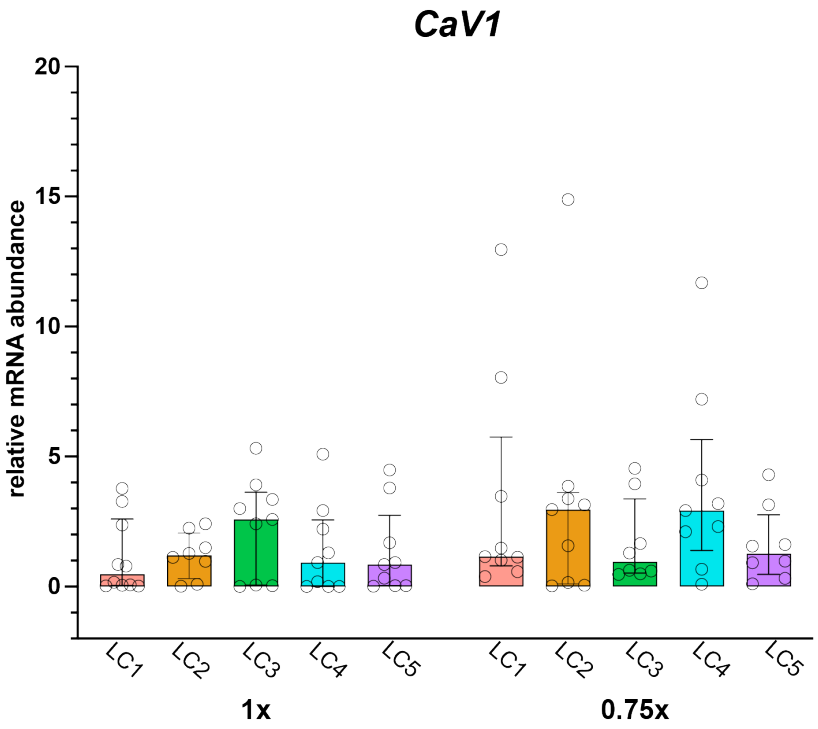

Figure 11. Effect of exposure to 0.75x saline for 24 h on the relative abundance of *CaV1* mRNA in the large cells of the cardiac ganglion. Boxplots displaying relative mRNA abundance in large cells (LC) 1-5 after 24 h in 1x saline and 0.75x saline. Each circle represents an individual neuron (*N*=8-10 for each LC type). Relative mRNA abundance was uniform across each LC in the 1x 24h control condition. No changes were observed across 1x and 0.75x in the LCs (Mann-Whitney *U* test, $p>0.05$; KS test, $p>0.05$). Bars represent the median value, and error bars represent interquartile range.

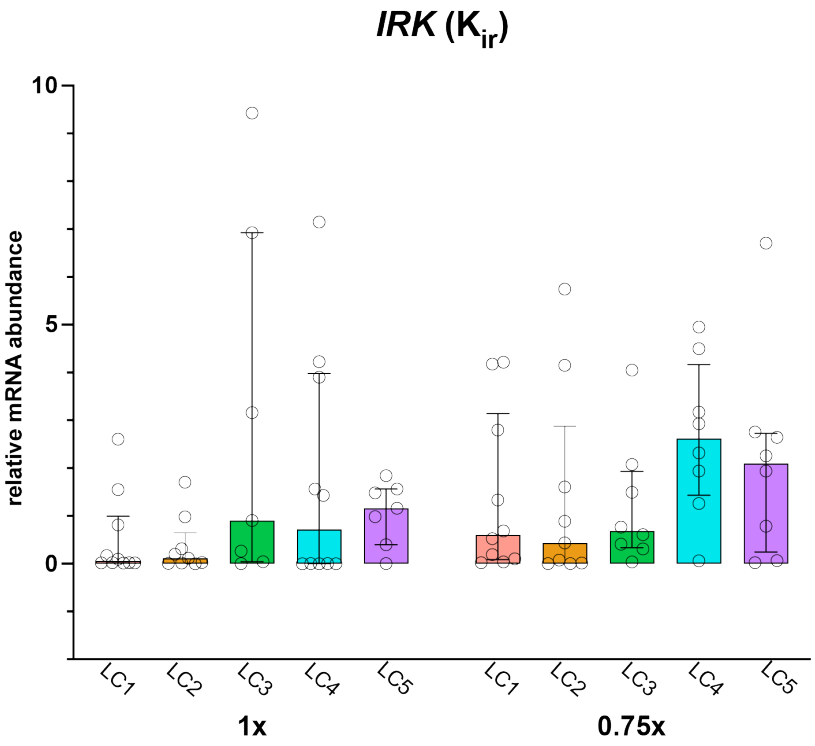

Figure 12. Effect of exposure to 0.75x saline for 24 h on the relative abundance of *IRK* mRNA in large cells of the cardiac ganglion. Boxplots displaying relative mRNA abundance in large cells (LC) 1-5 after 24 h in 1x saline and 0.75x saline. Each circle represents an individual neuron (*N*=8-10). Relative mRNA abundance was uniform across each LC in the 1x 24h control condition. No changes were observed across 1x and 0.75x conditions (Mann-Whitney *U* test, $p>0.05$; KS test, $p>0.05$). Bars represent the median value, and error bars represent interquartile range.

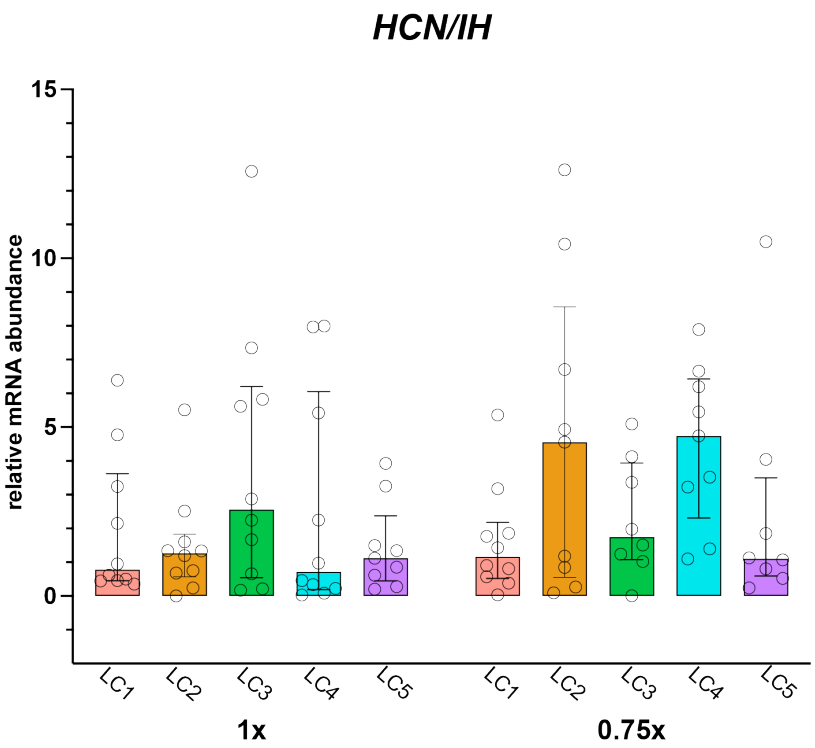

Figure 13. Effect of exposure to 0.75x saline for 24 h on the relative abundance of *HCN/IH* mRNA in large cells of the cardiac ganglion. Boxplots displaying relative mRNA abundance in large cells (LC) 1-5 after 24 h in 1x saline and 0.75x saline. Each circle represents an individual neuron (*N*=8-10). Relative mRNA abundance was uniform across each LC in the 1x 24h control condition. No changes were observed across 1x and 0.75x conditions (Mann-Whitney *U* test, $p>0.05$; KS test, $p>0.05$). Bars represent the median value, and error bars represent interquartile range.

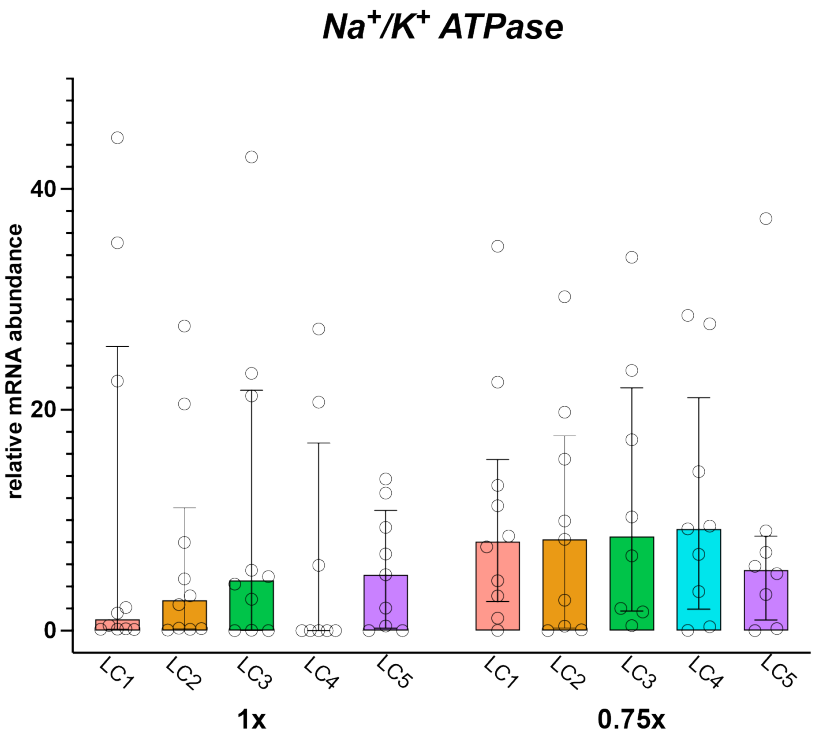

Figure 14. Effect of exposure to 0.75x saline for 24 h on the relative abundance of *Na⁺/K⁺-ATPase* mRNA in the large cells of the cardiac ganglion. Boxplots displaying relative mRNA abundance in large cells (LC) 1-5 after 24 h in 1x saline and 0.75x saline. Each circle represents an individual neuron (*N*=8-10). Relative mRNA abundance was uniform across each LC in the 1x 24h control condition. No changes were observed across 1x and 0.75x conditions (Mann-Whitney *U* test, $p>0.05$; KS test, $p>0.05$). Bars represent the median value, and error bars represent interquartile range.

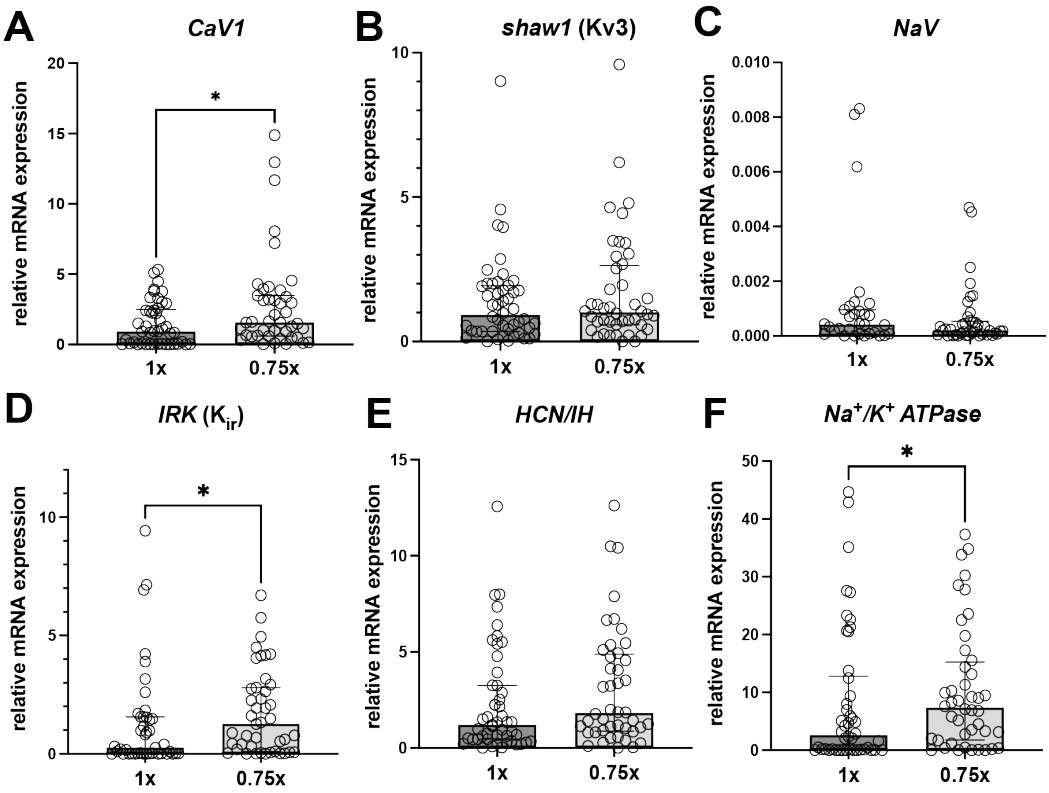

Figure 15. Effect of exposure to 0.75x saline for 24 h on the relative abundance of target mRNAs in the large cells of the cardiac ganglion. Boxplots displaying relative mRNA abundance in all large cells (LC 1-5) pooled together after 24 h in 1x saline and 0.75x saline. Each circle represents an individual neuron from one of the two conditions: *1x saline* (*N*=31-49) and *0.75x saline* (*N*=41-44).**(A)** *CaV1* mRNA abundances differed significantly between 1x and 0.75x groups (**p*<0.05, Mann-Whitney *U* test). **(B,C,E)** No changes were observed in relative mRNA expression between groups for *shaw1*, *NaV*, and *HCN/IH*. **(D)** Relative *IRK* mRNA abundances differed significantly between 1x and 0.75x groups (**p*< 0.05, Mann-Whitney *U* test). **(F)** Relative *Na+/K+ ATPase* mRNA abundances differed significantly between 1x and 0.75x groups (**p*<0.05, Mann-Whitney *U* test).

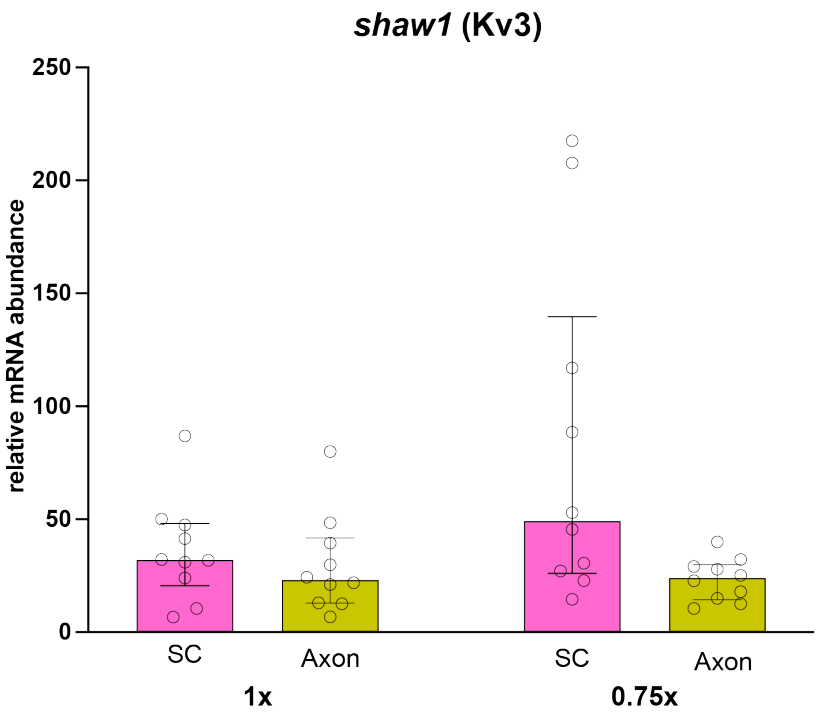

Figure 16. Effect of exposure to 0.75x saline for 24 h on the relative abundance of *shaw1* mRNA in the small cells of the cardiac ganglion. Boxplots displaying relative mRNA abundance in the small cells (SC) and a section of axon containing no cell bodies after 24 h in 1x or 0.75x saline (SC *N*=10; Axon *N*=10). No differences were observed between populations in 1x and 0.75x saline (Mann-Whitney *U* test, $p>0.05$; KS test, $p>0.05$). Bars represent the median value, and error bars represent interquartile range.

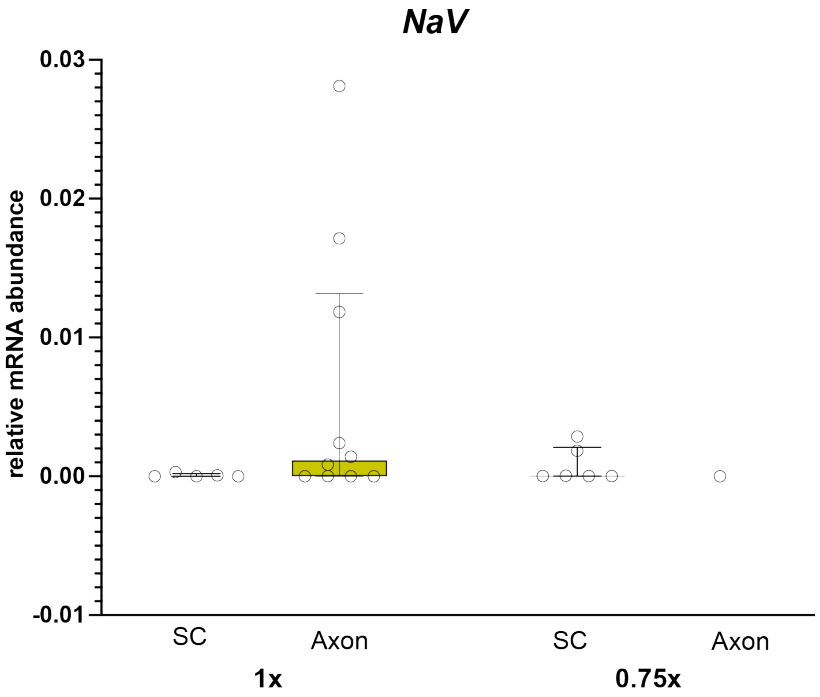

Figure 17. Effect of exposure to 0.75x saline for 24 h on the relative abundance of *NaV* mRNA in the small cells and axon of the cardiac ganglion. Boxplots displaying relative mRNA abundance in the small cells (SC) and a section of axon after 24 h in 1x or 0.75x saline (SC N=5-6, Axon 1x N=10, Axon 2x N=1). No differences were observed between populations in 1x and 0.75x saline (Mann-Whitney U test, p>0.05; KS test, p>0.05). Bars represent the median value, and error bars represent interquartile range.

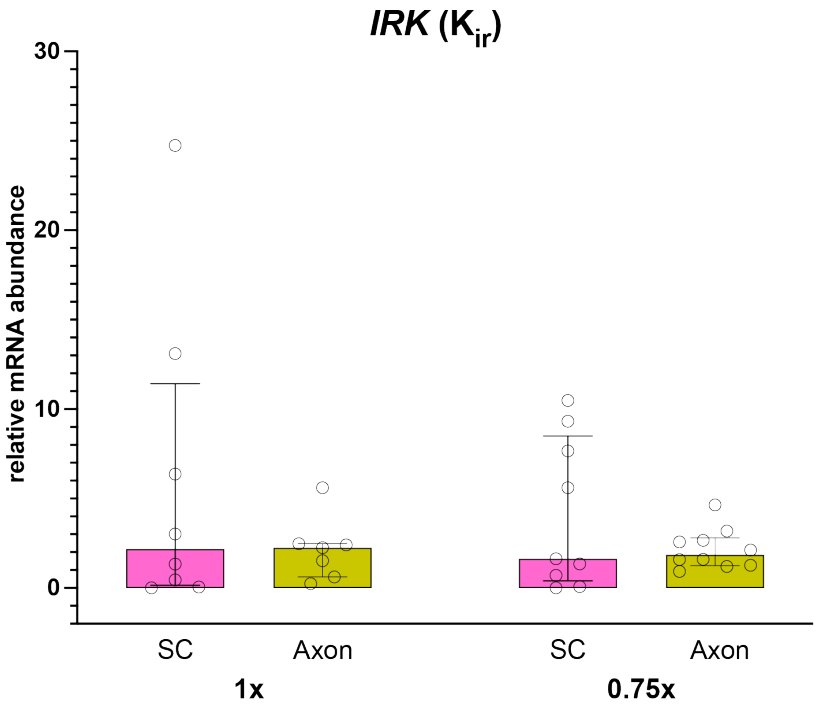

Figure 18. Effect of exposure to 0.75x saline for 24 h on the relative abundance of *IRK* mRNA in the smalls cells and axon of the cardiac ganglion. Boxplots displaying relative mRNA abundance in the small cells (SC) and a section of axon after 24 h in 1x or 0.75x saline (SC *N*=8-9; Axon *N*=7-10). No differences were observed between populations in 1x and 0.75x saline (Mann-Whitney *U* test, $p>0.05$; KS test, $p>0.05$). Bars represent the median value, and error bars represent interquartile range.

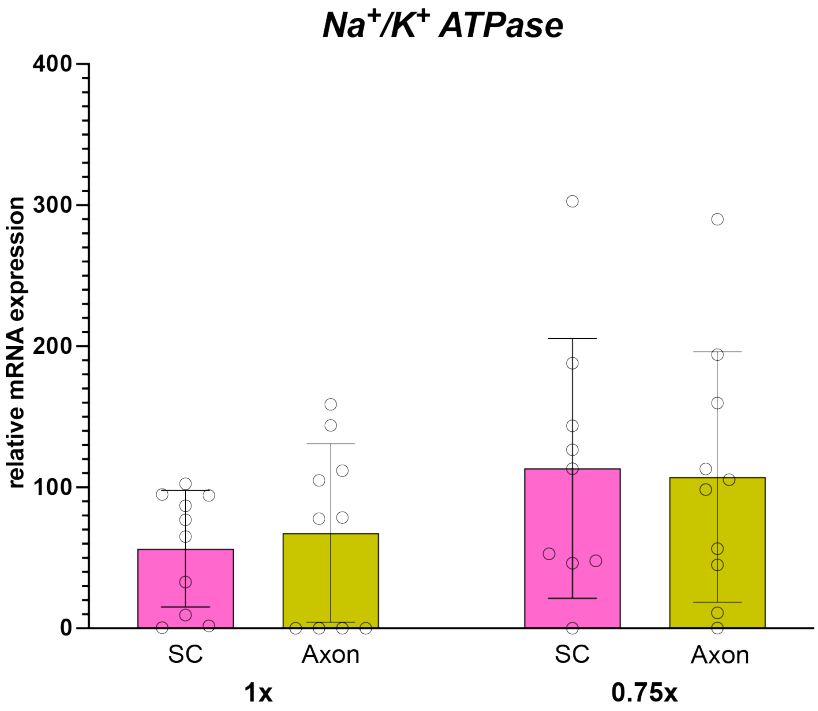

Figure 19. Effect of exposure to 0.75x saline for 24 h on the relative abundance of *Na⁺/K⁺-ATPase* mRNA in small cells and axon of the cardiac ganglion. Boxplots displaying relative mRNA abundance in the small cells (SC) and a section of axon after 24 h in 1x or 0.75x saline (SC *N*=8-10; Axon *N*=10). No differences were observed between the SC or Axon groups in 1x and 0.75x saline (Mann-Whitney *U* test, $p>0.05$; KS test, $p>0.05$). Bars represent the median value, and error bars represent interquartile range..

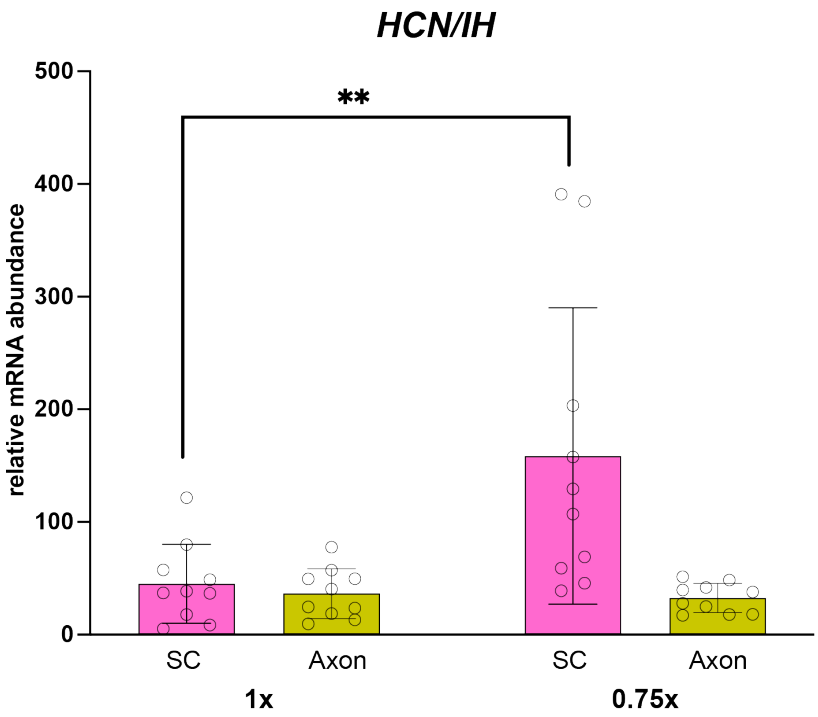

Figure 20. Effect of exposure to 0.75x saline for 24 h on the relative abundance of *HCN/IH* mRNA in the small cells and axon of the cardiac ganglion. Boxplots displaying relative mRNA abundance in the small cells (SC) and a section of axon after 24 h in 1x or 0.75x saline (SC N=10; Axon N=10). For the SC group, the distributions in 1x and 0.75x were significantly different (**p<0.05, Mann-Whitney U test). No differences were observed between the Axon groups in 1x and 0.75x saline. Bars represent the median value, and error bars represent interquartile range.

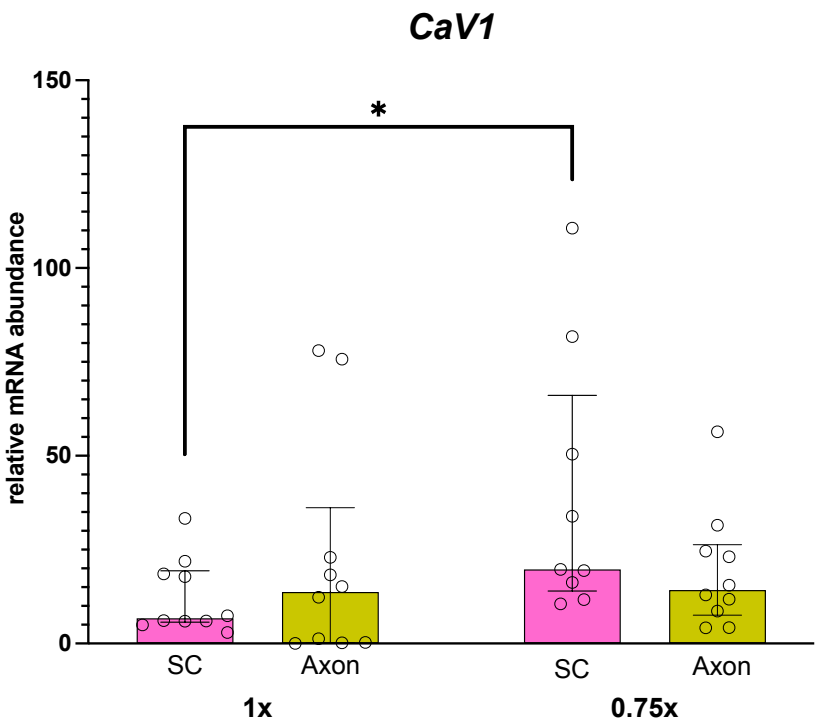

Figure 21. Effect of exposure to 0.75x saline for 24 h on the relative abundance of *CaV1* mRNA in small cells and axon of the cardiac ganglion. Boxplots displaying relative mRNA abundance in the small cells (SC) and a section of axon containing no cell bodies after 24 h in 1x or 0.75x saline (SC *N*=10; Axon *N*=10). For the SC group, the median values were significantly different between the two groups (Mann-Whitney *U* test, **p*<0.05). No differences were observed between axon populations in 1x and 0.75x saline. Bars represent the median value, and error bars represent interquartile range.

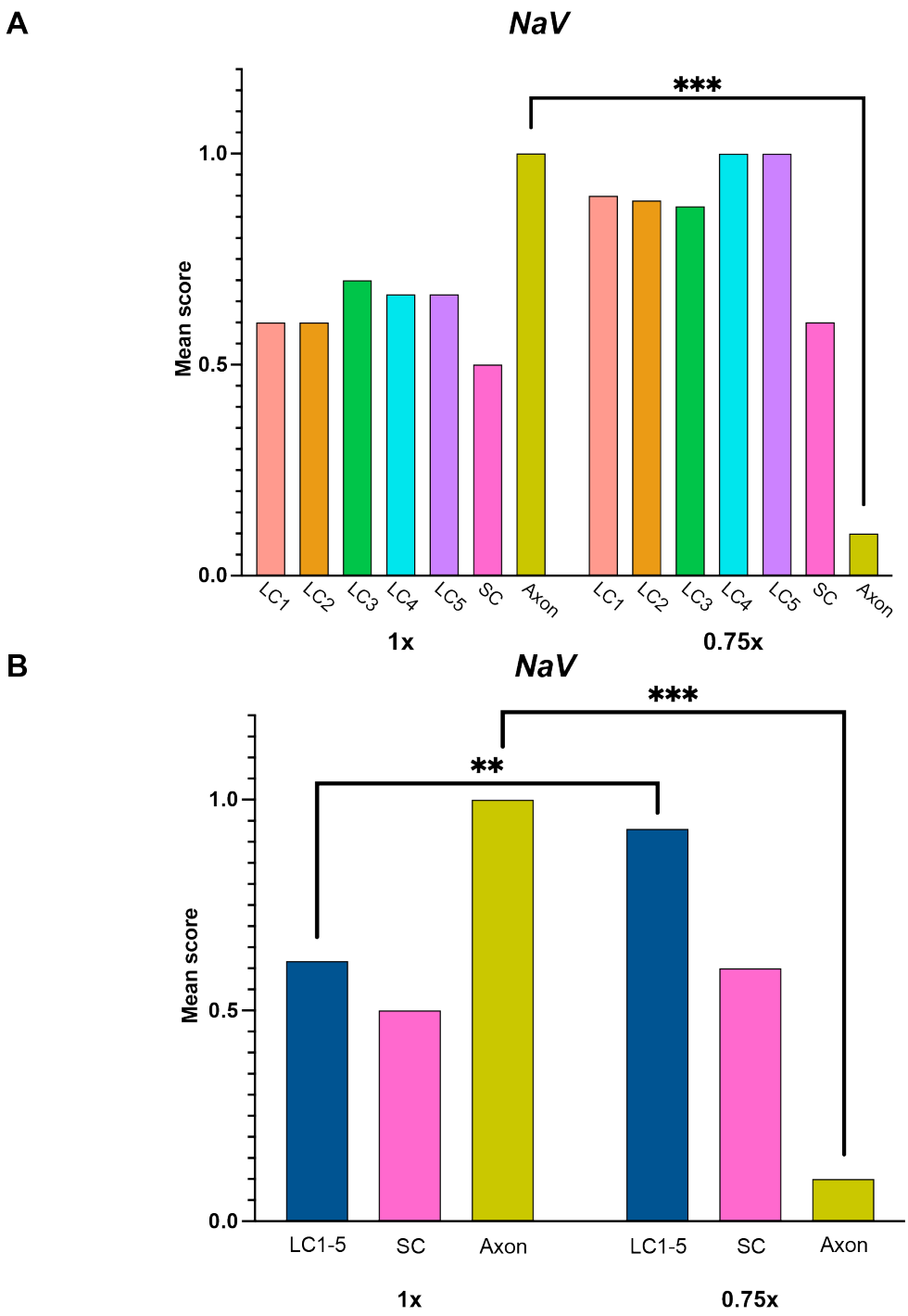

Figure 22. Presence of *NaV* mRNA increases in large cells and decreases in the axon after 24 h in 0.75x saline. A binomial scoring system was developed to assess changes in *NaV* transcript abundance with altered salinity. Individual samples within each sample type were assigned a value of either 0 or 1 based on whether detectable levels of *NaV* mRNA were present in the sample, with 0 indicating no expression and 1 indicating some level of expression. Bars represent the mean score for each sample type. **(A)** The results of a Fisher's exact test indicate a signficant association between saline condition and presence of transcript for axon samples (***p<0.001). (B) The results of a Fisher's exact test indicate a signficant association between saline condition and presence of transcript for pooled LC samples and axon samples (**p<0.01, ***p<0.001).

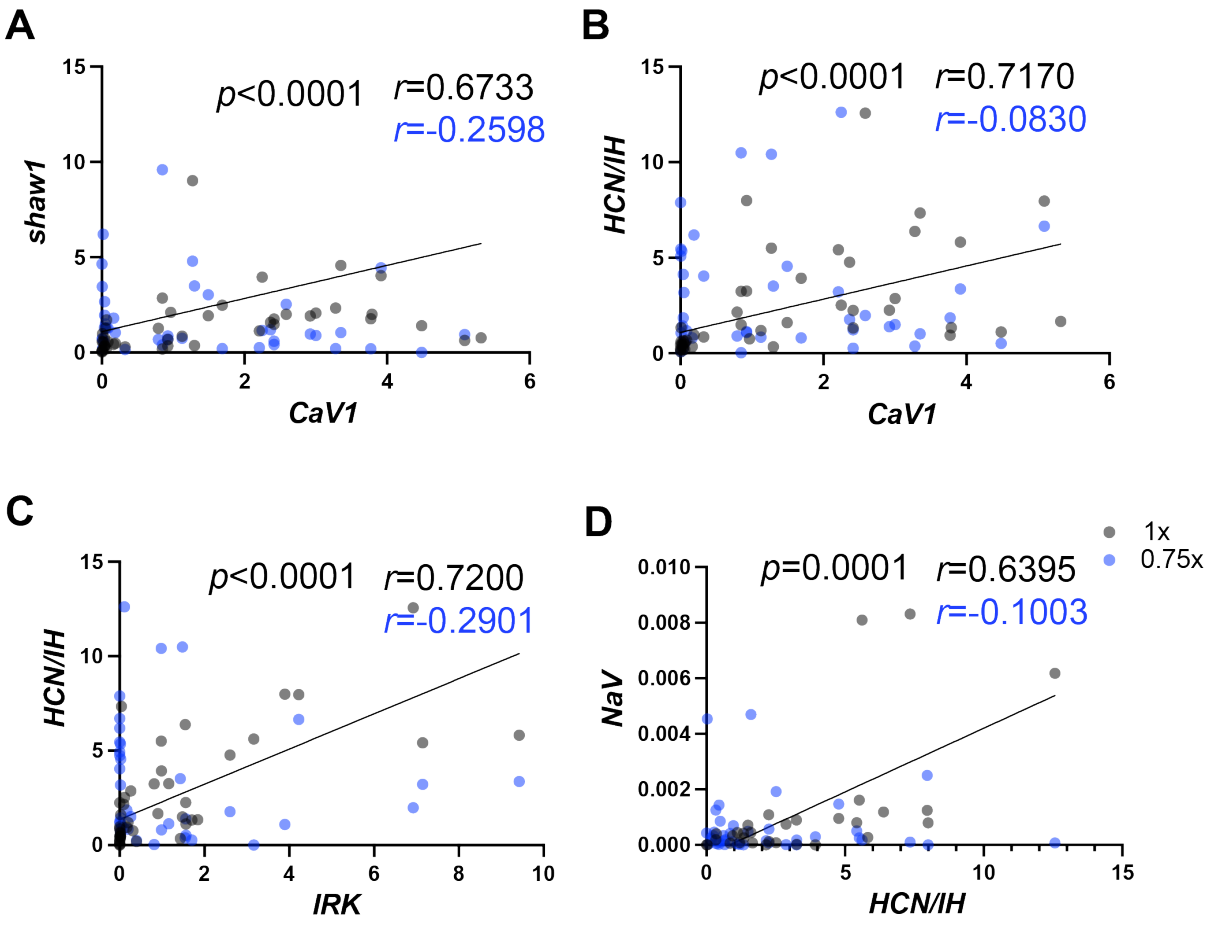

Figure 23. Ion channel mRNA relationships present in large cells after 24 h in 1x saline are lost with 24 h in 0.75x saline. Scatterplots of mRNA ion channel relationships for LC neurons in 1x saline (black) and 0.75x saline (blue) for 24 h. Each point represents one cell. Strong correlations (Spearman value > 0.6, $p<0.05$) are indicated by the plotting of a line of best fit.

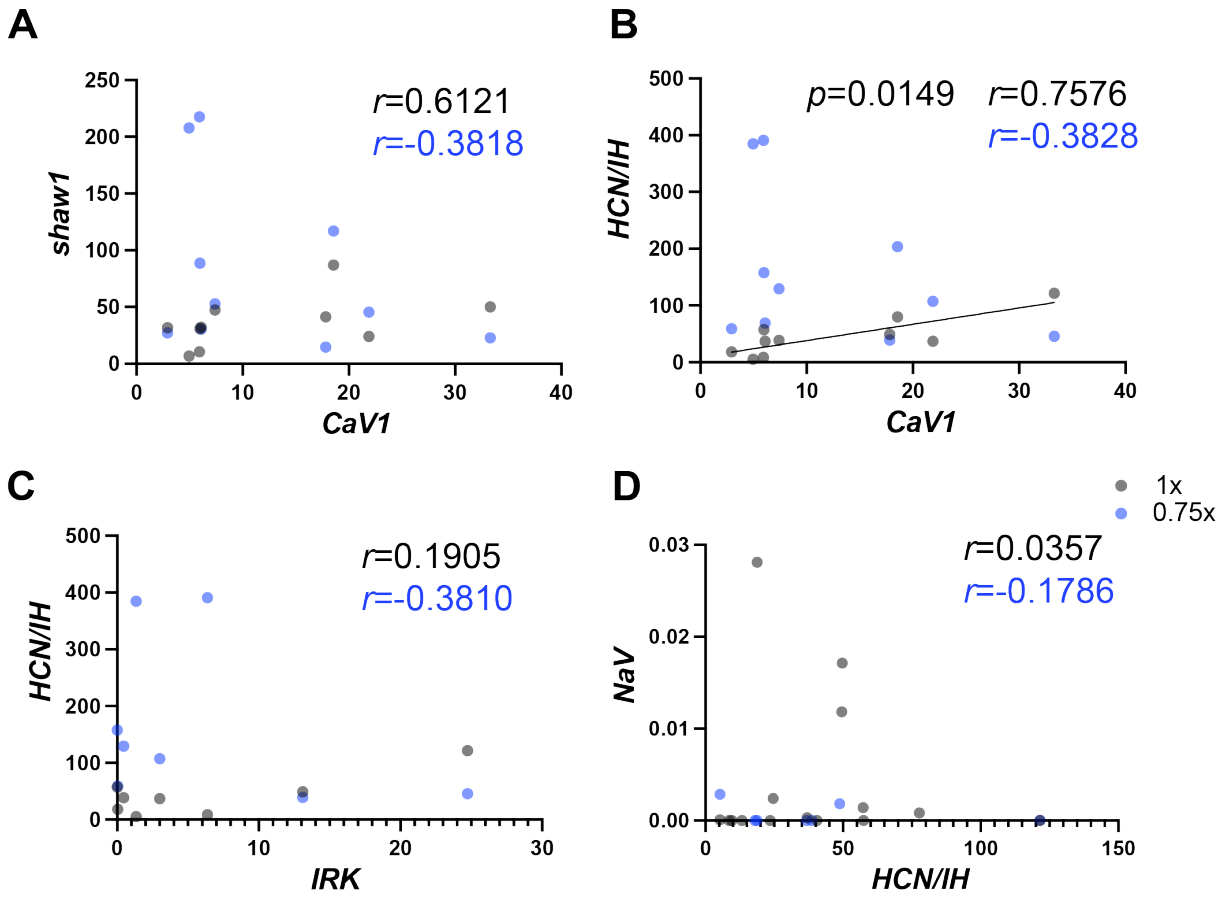

Figure 24. Ion channel mRNA relationships present in small cells after 24 h in 1x and 0.75x saline. Scatterplots of mRNA ion channel relationships for SC neurons in 1x saline (black) and 0.75x saline (blue) for 24 h. Each point represents one cell. Strong correlations (Spearman value > 0.6, $p<0.05$) are indicated by the plotting of a line of best fit.

REFERENCES

Alonso, L. M., & Marder, E. (2019). Visualization of currents in neural models with similar behavior and different conductance densities. *eLife*, *8*, e42722. https://doi.org/10.7554/eLife.42722

Alonso, L. M., & Marder, E. (2020). Temperature compensation in a small rhythmic circuit. *eLife*, *9*, e55470. https://doi.org/10.7554/eLife.55470

Baines R. A. (2005). Neuronal homeostasis through translational control. *Molecular neurobiology*, *32*(2), 113–121. https://doi.org/10.1385/MN:32:2:113

Bucher, D., Prinz, A. A., & Marder, E. (2005). Animal-to-animal variability in motor pattern production in adults and during growth. *The Journal of neuroscience : the official journal of the Society for Neuroscience*, *25*(7), 1611–1619. https://doi.org/10.1523/JNEUROSCI.3679-04.2005

Davis, G. W., & Goodman, C. S. (1998). Synapse-specific control of synaptic efficacy at the terminals of a single neuron. *Nature*, *392*(6671), 82–86. https://doi.org/10.1038/32176

Delcomyn F. (1980). Neural basis of rhythmic behavior in animals. *Science (New York, N.Y.)*, *210*(4469), 492–498. https://doi.org/10.1126/science.7423199

Desai, N. S., Rutherford, L. C., & Turrigiano, G. G. (1999). Plasticity in the intrinsic excitability of cortical pyramidal neurons. *Nature neuroscience*, *2*(6), 515–520. https://doi.org/10.1038/9165

Drion, G., O'Leary, T., & Marder, E. (2015). Ion channel degeneracy enables robust and tunable neuronal firing rates. Proceedings of the National Academy of Sciences of the United States of America, 112(38), E5361–E5370. https://doi.org/10.1073/pnas.1516400112

Finkbeiner, S., & Greenberg, M. E. (1998). Ca2+ channel-regulated neuronal gene expression. *Journal of neurobiology*, *37*(1), 171–189.

Goaillard, J. M., & Marder, E. (2021). Ion Channel Degeneracy, Variability, and Covariation in Neuron and Circuit Resilience. *Annual review of neuroscience*, *44*, 335–357. https://doi.org/10.1146/annurev-neuro-092920-121538

Golowasch, J., Buchholtz, F., Epstein, I. R., & Marder, E. (1992). Contribution of individual ionic currents to activity of a model stomatogastric ganglion neuron. *Journal of neurophysiology*, *67*(2), 341–349. https://doi.org/10.1152/jn.1992.67.2.341

Goulding M. (2009). Circuits controlling vertebrate locomotion: moving in a new direction. *Nature reviews. Neuroscience*, *10*(7), 507–518. https://doi.org/10.1038/nrn2608

Haddad, S. A., & Marder, E. (2018). Circuit Robustness to Temperature Perturbation Is Altered by Neuromodulators. *Neuron*, *100*(3), 609–623.e3. https://doi.org/10.1016/j.neuron.2018.08.035

Haley, J. A., Hampton, D., & Marder, E. (2018). Two central pattern generators from the crab, *Cancer borealis,* respond robustly and differentially to extreme extracellular pH. *eLife*, *7*, e41877. https://doi.org/10.7554/eLife.41877

He, L. S., Rue, M. C. P., Morozova, E. O., Powell, D. J., James, E. J., Kar, M., & Marder, E. (2020). Rapid adaptation to elevated extracellular potassium in the pyloric circuit of the crab, *Cancer borealis*. *Journal of neurophysiology*, *123*(5), 2075–2089. https://doi.org/10.1152/jn.00135.2020

https://doi.org/10.1016/j.cophys.2018.01.006

Lin, W. H., Günay, C., Marley, R., Prinz, A. A., & Baines, R. A. (2012). Activity-dependent alternative splicing increases persistent sodium current and promotes seizure. *The*

Journal of neuroscience : the official journal of the Society for Neuroscience, *32*(21), 7267–7277. https://doi.org/10.1523/JNEUROSCI.6042-11.2012

Lipscombe, D., Allen, S. E., & Toro, C. P. (2013). Control of neuronal voltage-gated calcium ion channels from RNA to protein. *Trends in neurosciences*, *36*(10), 598–609. https://doi.org/10.1016/j.tins.2013.06.008

Marder, E., & Bucher, D. (2001). Central pattern generators and the control of rhythmic movements. *Current biology : CB*, *11*(23), R986–R996. https://doi.org/10.1016/s0960-9822(01)00581-4

Marder, E., & Bucher, D. (2007). Understanding circuit dynamics using the stomatogastric nervous system of lobsters and crabs. *Annual review of physiology*, *69*, 291–316. https://doi.org/10.1146/annurev.physiol.69.031905.161516

Marder, E., & Prinz, A. A. (2002). Modeling stability in neuron and network function: the role of activity in homeostasis. *BioEssays : news and reviews in molecular, cellular and developmental biology*, *24*(12), 1145–1154. https://doi.org/10.1002/bies.10185

Marder, E., & Prinz, A. A. (2003). Current compensation in neuronal homeostasis. *Neuron*, *37*(1), 2–4. https://doi.org/10.1016/s0896-6273(02)01173-x

Marom, S., & Marder, E. (2023). A biophysical perspective on the resilience of neuronal excitability across timescales. *Nature reviews. Neuroscience*, *24*(10), 640–652. https://doi.org/10.1038/s41583-023-00730-9

Mermelstein, P. G., Bito, H., Deisseroth, K., & Tsien, R. W. (2000). Critical dependence of cAMP response element-binding protein phosphorylation on L-type calcium channels supports a selective response to EPSPs in preference to action potentials. *The Journal of neuroscience : the official journal of the Society for Neuroscience*, *20*(1), 266–273. https://doi.org/10.1523/JNEUROSCI.20-01-00266.2000

Norris, B. J., Wenning, A., Wright, T. M., & Calabrese, R. L. (2011). Constancy and variability in the output of a central pattern generator. *The Journal of neuroscience : the official journal of the Society for Neuroscience*, *31*(12), 4663–4674. https://doi.org/10.1523/JNEUROSCI.5072-10.2011

Northcutt, A. J., & Schulz, D. J. (2020). Molecular mechanisms of homeostatic plasticity in central pattern generator networks. *Developmental neurobiology*, *80*(1-2), 58–69. https://doi.org/10.1002/dneu.22727

Northcutt, A. J., Kick, D. R., Otopalik, A. G., Goetz, B. M., Harris, R. M., Santin, J. M., Hofmann, H. A., Marder, E., & Schulz, D. J. (2019). Molecular profiling of single neurons of known identity in two ganglia from the crab *Cancer borealis*. *Proceedings of the National Academy of Sciences of the United States of America*, *116*(52), 26980–26990. https://doi.org/10.1073/pnas.1911413116

Northcutt, A. J., Lett, K. M., Garcia, V. B., Diester, C. M., Lane, B. J., Marder, E., & Schulz, D. J. (2016). Deep sequencing of transcriptomes from the nervous systems of two decapod crustaceans to characterize genes important for neural circuit function and modulation. *BMC genomics*, *17*(1), 868. https://doi.org/10.1186/s12864-016-3215-z

O'Leary, T., & Marder, E. (2016). Temperature-Robust Neural Function from Activity-Dependent Ion Channel Regulation. Current biology : CB, 26(21), 2935–2941. https://doi.org/10.1016/j.cub.2016.08.061

O'Leary, T., Williams, A. H., Caplan, J. S., & Marder, E. (2013). Correlations in ion channel expression emerge from homeostatic tuning rules. *Proceedings of the National Academy*

of Sciences of the United States of America, *110*(28), E2645–E2654. https://doi.org/10.1073/pnas.1309966110

O'Leary, T., Williams, A. H., Franci, A., & Marder, E. (2014). Cell types, network homeostasis, and pathological compensation from a biologically plausible ion channel expression model. *Neuron*, *82*(4), 809–821. https://doi.org/10.1016/j.neuron.2014.04.002

O'Leary, T. (2018) Homeostasis, Failure of Homeostasis and Degenerate Ion Channel Regulation. *Current Opinion in Physiology*, 2, 129-138.

Paradis, S., Sweeney, S. T., & Davis, G. W. (2001). Homeostatic control of presynaptic release is triggered by postsynaptic membrane depolarization. *Neuron*, *30*(3), 737–749. https://doi.org/10.1016/s0896-6273(01)00326-9

Prinz, A. A., Bucher, D., & Marder, E. (2004). Similar network activity from disparate circuit parameters. *Nature neuroscience*, *7*(12), 1345–1352. https://doi.org/10.1038/nn1352

Ransdell, J. L., Faust, T. B., & Schulz, D. J. (2010). Correlated Levels of mRNA and Soma Size in Single Identified Neurons: Evidence for Compartment-specific Regulation of Gene Expression. *Frontiers in molecular neuroscience*, *3*, 116. https://doi.org/10.3389/fnmol.2010.00116

Ratliff, J., Franci, A., Marder, E., & O'Leary, T. (2021). Neuronal oscillator robustness to multiple global perturbations. *Biophysical journal*, *120*(8), 1454–1468. https://doi.org/10.1016/j.bpj.2021.01.038

Rinberg, A., Taylor, A. L., & Marder, E. (2013). The effects of temperature on the stability of a neuronal oscillator. *PLoS computational biology*, *9*(1), e1002857. https://doi.org/10.1371/journal.pcbi.1002857

Schulz, D. J., Goaillard, J. M., & Marder, E. (2006). Variable channel expression in identified single and electrically coupled neurons in different animals. *Nature neuroscience*, *9*(3), 356–362. https://doi.org/10.1038/nn1639

Schulz, D. J., Goaillard, J. M., & Marder, E. E. (2007). Quantitative expression profiling of identified neurons reveals cell-specific constraints on highly variable levels of gene expression. *Proceedings of the National Academy of Sciences of the United States of America*, *104*(32), 13187–13191. https://doi.org/10.1073/pnas.0705827104

Schneider, A. C., Itani, O., Bucher, D., & Nadim, F. (2022). Neuromodulation reduces interindividual variability of neuronal output. *eNeuro*, *9*(4), ENEURO.0166-22.2022. Advance online publication. https://doi.org/10.1523/ENEURO.0166-22.2022

Soofi, W., Goeritz, M. L., Kispersky, T. J., Prinz, A. A., Marder, E., & Stein, W. (2014). Phase maintenance in a rhythmic motor pattern during temperature changes in vivo. *Journal of neurophysiology*, *111*(12), 2603–2613. https://doi.org/10.1152/jn.00906.2013

Swensen, A. M., & Bean, B. P. (2005). Robustness of burst firing in dissociated purkinje neurons with acute or long-term reductions in sodium conductance. *The Journal of neuroscience : the official journal of the Society for Neuroscience*, *25*(14), 3509–3520. https://doi.org/10.1523/JNEUROSCI.3929-04.2005

Tang, L. S., Goeritz, M. L., Caplan, J. S., Taylor, A. L., Fisek, M., & Marder, E. (2010). Precise temperature compensation of phase in a rhythmic motor pattern. *PLoS biology*, *8*(8), e1000469. https://doi.org/10.1371/journal.pbio.1000469

Tang, L. S., Taylor, A. L., Rinberg, A., & Marder, E. (2012). Robustness of a rhythmic circuit to short- and long-term temperature changes. *The Journal of neuroscience : the official journal of the Society for Neuroscience*, *32*(29), 10075–10085. https://doi.org/10.1523/JNEUROSCI.1443-12.2012

Tanner, M. R., & Beeton, C. (2018). Differences in ion channel phenotype and function between humans and animal models. *Frontiers in bioscience (Landmark edition)*, *23*(1), 43–64. https://doi.org/10.2741/4581

Tazaki, K., & Cooke I. M. (1983). Separation of neuronal sites of driver potential and impulse generation by ligaturing in the cardiac ganglion of the lobster, *Homarus americanus*. *Journal of Comparative Physiology*, *151*, 329–346. https://doi.org/10.1007/BF00623908

Temporal, S., Desai, M., Khorkova, O., Varghese, G., Dai, A., Schulz, D. J., & Golowasch, J. (2012). Neuromodulation independently determines correlated channel expression and conductance levels in motor neurons of the stomatogastric ganglion. *Journal of neurophysiology*, *107*(2), 718–727. https://doi.org/10.1152/jn.00622.2011

Tobin, A. E., Cruz-Bermúdez, N. D., Marder, E., & Schulz, D. J. (2009). Correlations in ion channel mRNA in rhythmically active neurons. *PloS one*, *4*(8), e6742. https://doi.org/10.1371/journal.pone.0006742

Turrigiano, G. G., & Nelson, S. B. (2004). Homeostatic plasticity in the developing nervous system. *Nature reviews. Neuroscience*, *5*(2), 97–107. https://doi.org/10.1038/nrn1327

Wheeler, D. G., Groth, R. D., Ma, H., Barrett, C. F., Owen, S. F., Safa, P., & Tsien, R. W. (2012). Ca(V)1 and Ca(V)2 channels engage distinct modes of Ca(2+) signaling to control CREB-dependent gene expression. *Cell*, *149*(5), 1112–1124. https://doi.org/10.1016/j.cell.2012.03.041

Zhao, S., & Golowasch, J. (2012). Ionic current correlations underlie the global tuning of large numbers of neuronal activity attributes. *The Journal of neuroscience : the official journal of the Society for Neuroscience*, *32*(39), 13380–13388. https://doi.org/10.1523/JNEUROSCI.6500-11.2012